




Review

Nb₂CT_x-Based MXenes Most Recent Developments: From Principles to New Applications

Tholkappiyan Ramachandran ^{1,2}, Abdel-Hamid Ismail Mourad ^{1,2,3,*} and Mostafa S. A. ElSayed ^{1,4,*}

¹ Department of Mechanical and Aerospace Engineering, College of Engineering, United Arab Emirates University, Al Ain P.O. Box 15551, United Arab Emirates; t_ramachandran@uaeu.ac.ae

² National Water and Energy Center, United Arab Emirates University, Al Ain P.O. Box 15551, United Arab Emirates

³ Mechanical Design Department, Faculty of Engineering, Helwan University, Cairo 11795, Egypt

⁴ Department of Mechanical and Aerospace Engineering, Carleton University, Ottawa, ON K1S 5B6, Canada

* Correspondence: ahmourad@uaeu.ac.ae (A.-H.I.M.); mostafa.elsayed@carleton.ca or mselsayed@uaeu.ac.ae (M.S.A.E.)

Abstract: MXenes are progressively evolving two-dimensional (2D) materials with an expanding wide range of applications in the field of energy storage. They rank among the best electrode materials for cutting-edge energy storage systems. Energy storage device performance is greatly enhanced by MXenes and their composite materials. As technology has improved over the last several decades, the demand for high-capacity energy storage devices that are versatile, sturdy, and have cheap production costs has increased. MXene, which is based on Nb₂CT_x, is the most current material to emerge for energy storage applications. Nb₂CT_x MXene is now the most sought-after material in the 2D family due to its flexibility, high conductivity, superior electrochemical nature, superior hydrophilicity, tunable surface functional groups, great mechanical properties, and 2D layered structure. Examples include gas and biosensors, water splitting, water purification, antimicrobial coatings, electromagnetic interference shielding, and transparent electrical conductors. Because of the distinctive properties of Nb₂CT_x MXene, scientists are working on further theoretical and experimental enhancements. The objective of this work is to deliver an outline of current breakthroughs in Nb₂CT_x MXene for the construction of robust, flexible, and highly effective electrochemical energy storage devices powered by supercapacitors. Deep research has been conducted on the structure of Nb₂CT_x MXene, as well as on different synthesis techniques and their distinctive properties. The emphasis has also been placed on how various aspects, such as electrode architecture design, electrolyte composition, and so on, influence the charge storage device and electrochemical efficiency of Nb₂CT_x MXene-based supercapacitors. This article also discusses the most recent advancements in Nb₂CT_x MXene composite-based supercapacitors.

Keywords: Nb₂CT_x MXene; prospective properties; biological; sensors; energy storage



Citation: Ramachandran, T.; Mourad, A.-H.I.; ElSayed, M.S.A. Nb₂CT_x-Based MXenes Most Recent Developments: From Principles to New Applications. *Energies* **2023**, *16*, 3520. <https://doi.org/10.3390/en16083520>

Academic Editor: Cai Shen

Received: 25 January 2023

Revised: 23 February 2023

Accepted: 13 April 2023

Published: 18 April 2023



Copyright: © 2023 by the authors. Licensee MDPI, Basel, Switzerland. This article is an open access article distributed under the terms and conditions of the Creative Commons Attribution (CC BY) license (<https://creativecommons.org/licenses/by/4.0/>).

1. Introduction

Since the finding of single-layer graphene oxide (GO's) extraordinary physical characteristics a few years ago, two-dimensional (2D) materials have been actively explored. This piqued our curiosity, leading to a new study on well-known 2D materials including metal dichalcogenides and boron nitride, as well as the discovery of several novel 2D materials. Although many of these materials remain solely academic, others have acquired prominence owing to their enticing qualities, leading to practical applications. MXenes (pronounced “maxenes”) are transition metal carbides and nitrides, a rapidly growing family of 2D materials. M_{n+1}X_nT_x is the formula for a typical 2D flake of MXene, which has n + 1 (n = 1–3) layers of early transition metals (M) interspersed with n layers of carbon or nitrogen. Surface terminations, such as hydroxyl, oxygen, chlorine, or fluorine, that are attached to the outer M layers are represented by the symbol T_x in the formula, and n is the

number [1,2]. Figure 1 shows the overview of 2D Nb₂CT_x MXene and their applications, presented through blowing bubbles art.

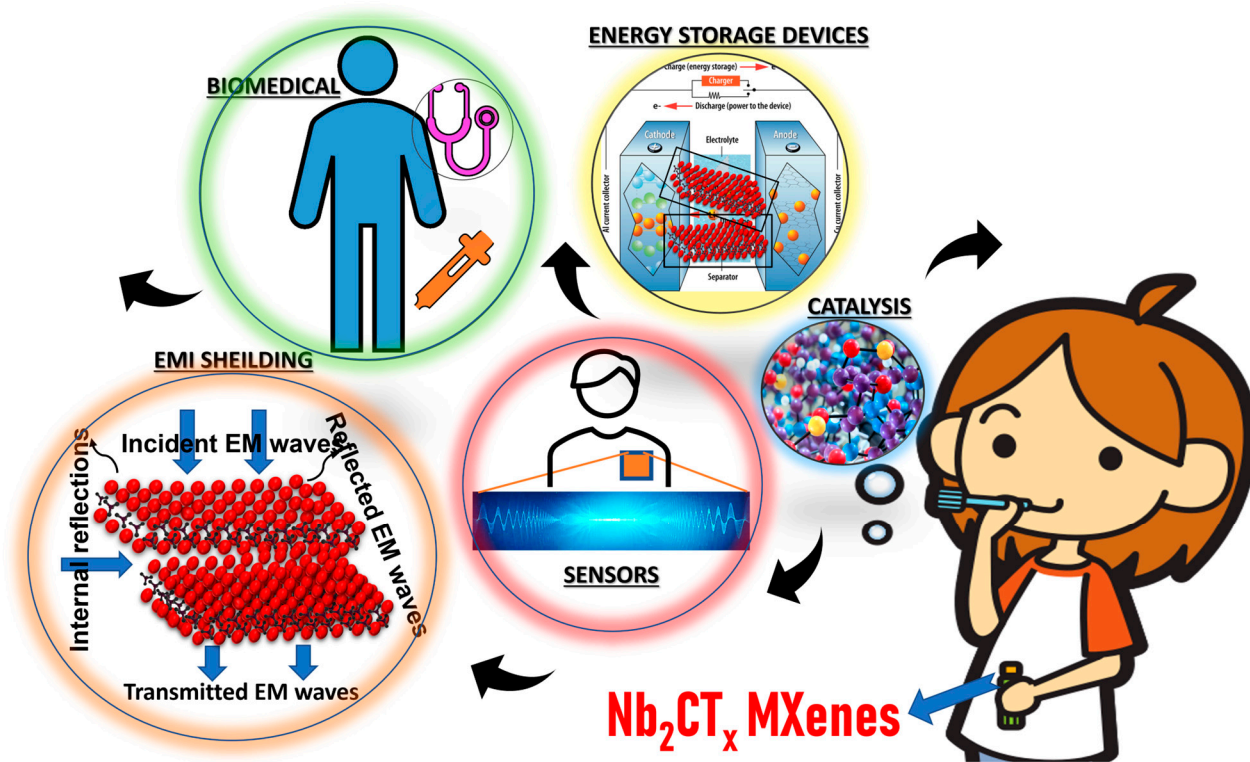


Figure 1. The overview of 2D Nb₂CT_x MXene and their applications, presented through blowing bubbles art.

Comprehensive explanations of the preparation process, behavior, and structures of several MXene compounds are discussed in many reviews [3–5]. Numerous MXene-based composites are also listed, along with examples of how they are used in the most recent supercapacitor fabrication processes. This paper covers the most current advancements in Nb₂CT_x MXene’s electrochemical performance in supercapacitor devices. Nb₂CT_x MXene has rapidly advanced in the area of energy storage applications since 2015, and numerous articles for supercapacitor research have been published. For instance, when discussing Nb₂CT_x MXene for sodium-ion batteries, Zhang et al. [6] compared differences between experimental and theoretical findings in excellent electrochemical behavior. Long et al. [7] described Nb₂CT_x MXene in numerous power storage systems and discussed some of its issues. Nb₂CT_x MXene is presented by Wu et al. [8] in potassium ion batteries and its method of potassium storage is described. Nasrin et al. [9] further discuss the development of 2D/2D MXene heterostructures on the functionality of supercapacitors, MXenes production, stacking, and physical properties. Qiuni Zhao et al. developed a neuron-like composite film based on Nb₂CT_x/sodium alginate by electrospinning for power generation and humidity sensing [10]. Weijing Zhao et al. designed a stretchable, adhesive, and conductive MXene-polyacrylic acid hydrogel by a simple pre-crosslinking method followed by successive direct ink writing 3D printing [11]. However, the literature still lacks a comprehensive review of the use of niobium MXenes. Hence, in this overview, we examined the fabrication of 2D-based Nb₂CT_x MXs techniques, their prospective properties, and their considerable use in energy storage devices, biological, sensors, electromagnetic interference (EMI) shielding, microwave absorptions, and catalysis applications [12]. This review also offers directions on the prospects for Nb₂CT_x MXene design for energy storage; composites for storing energy are presented and predicted.

2. Synthetic Approach for Nb₂CT_x

Since the discovery of the MXene, numerous synthesis techniques have been created and envisioned for both new and old MXenes that require further optimization. There are two main categories of synthesis top-down and bottom-up approaches, which are essentially etching-based and non-etching-based synthesis of MXene, respectively. The unique characteristics, such as excellent charge-discharge rates, conductivity, biocompatibility, and high photothermal stability, of Nb₂CT_x MXene are closely correlated with the synthesis procedures, which have a substantial impact on its chemical environment, electrical conductivity, flaws, lateral flake size, etching effectiveness and surface terminations [13]. Since Gogotsi's team produced MXene in 2011 for the first time, extensive research has been performed on creating new MAX phases and etching other MXenes, which have a flake-like shape [14]. Figure 2 shows the story of MXenes synthesis concerning year [14].

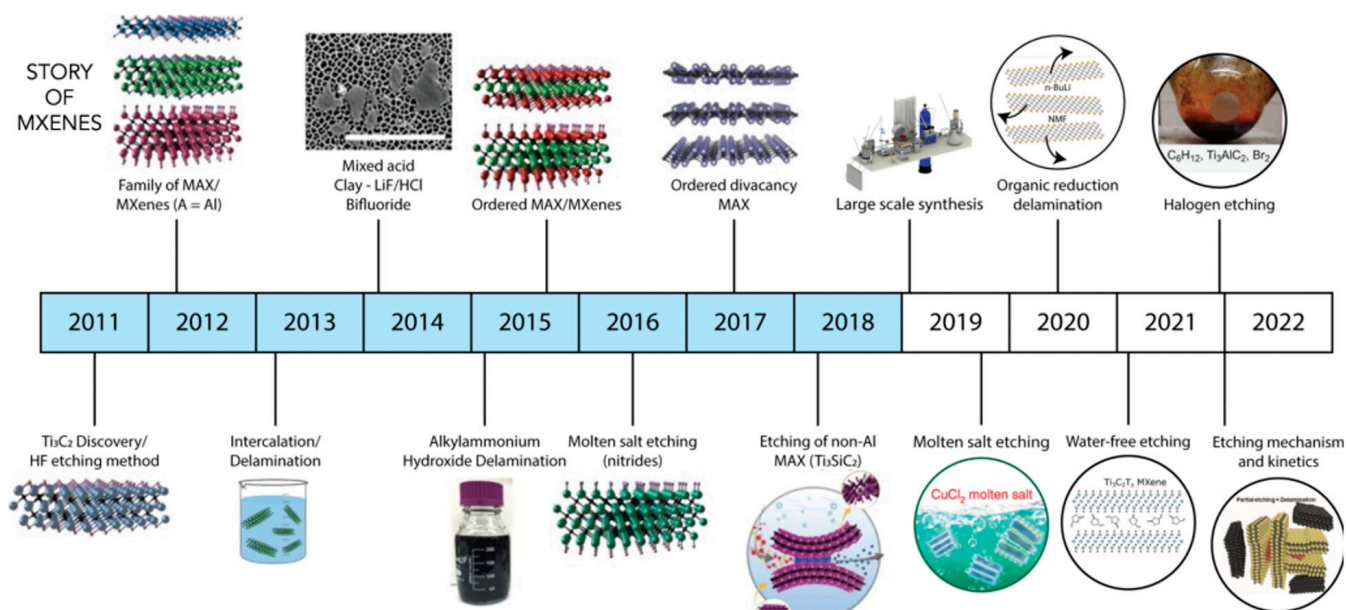
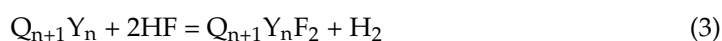
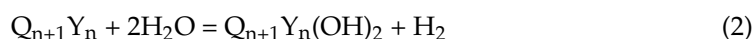
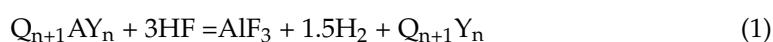


Figure 2. Story of MXenes synthesis concerning year. Reprinted with permission from Ref. [14].

Most MXs have so far been created by simultaneously carving Al from the MAX phase using HF as the etchant. Due to HF's severe toxicity, alternate methods using hardly hazardous etchants, such as a combination of HCL and LiF, have been used to successfully etch the A component. Together with other 2D materials, the study of MX sources is still in its infancy, which gives them a significant impact on new applications.

2.1. By HF Etching

The most often employed approach has been identified to be selective wet chemical etching of chemically active "A" layers from the precursor MAX phase material. The process of breaking the strong chemical reactions between both components A and M of their source MAX phase materials when HF is used as the etchant may be summed up as the following chemical reactions:



Reaction (1) demonstrates how the A elements are removed from the MAX phase to produce the $Q_{n+1}Y_n$ phase. The functionalization stages of exposed titanium surfaces ended by -OH and/or -F are described in reactions (2) and (3). As Q–A bindings in the MAX phase are weaker than Q–Y bonds, etching processes of A components from the MAX stage can exist in aqueous HF. Huang et al. stated that the formation of few-layer Nb_2CT_x from the Nb_2AlC fine particles (400 mesh) were mixed with 50% concentrated HF solution and aqueous KOH solution (5 mL, 10 wt%) to transform -OH into -O at 300–600 °C in Ar atmosphere [15]. Ni-decorated Nb_2C MXene was studied by Zhu et al. through an etching method using HF solution (40 wt%) [16]. Pandey et al. synthesized Nb_2CT_x and $Nb_4C_3T_x$ MXenes using 48–51% HF aqueous solution by probe sonication with different lateral sizes [17]. For Bulk- Nb_2CT_x , MXene was fabricated through Nb_2AlC MAX powders with 48% concentrated HF acid at 55 °C and single-layered Nb_2CT_x MXene using TMAOH solution, as reported by Jiahui Li et al. [18]. Gul et al. reported 2D Nb_2C and Erbium (Er) adsorbed MXene, produced by wet-chemical etching method in conc. (HF-50%) [19]. In 2022, Kumar and Pal synthesized Nb_2CT_x MXene from the Nb_2AlC in 10 mL of HF-48% at 55 °C [20]. According to Zong et al., flower-petal-like Nb_2C MXene with MoS_2 was synthesized using 35 wt.% hydrofluoric acids followed by the hydrothermal method [21]. A sandwich-like N-doped $CNT@Nb_2C$ MXene composite was reported by Zhang et al. using hydrofluoric acid (HF, 40%) [22]. Byeon et al. reported the Nb_2CT_x -CNT composite was etched in 50% hydrofluoric acid [23]. Zhou et al. synthesized the MXene Nb_2C from mesh MAX powder and added it to 49 wt% hydrofluoric acid solution at 60 °C for 48 h [24]. Nb_2CT_x MXene was successfully synthesized by Yan et al. via etching Nb_2AlC with hydrofluoric acid [25]. Niobium carbide (Nb_2CT_x) MXene was prepared by Liu et al. via HF-49% at 55 °C for 48 h followed by tetramethylammonium hydroxide [26]. Nasrin et al. synthesized Ti_3C_2 MXene by selectively etching the MAX phase with a 48 wt.% HF solution [27]. Table 1 lists the several etching methods that were employed to produce Nb_2CT_x and $Nb_4C_3T_x$ MXenes using direct HF.

The HF-etching approach is simple and easily scalable for Nb_2CT_x preparation. However, using strong HF as the etchant is exceedingly dangerous, which limits its practical applicability. As a result, developing safer and more environmentally friendly etchants for the manufacture of Nb_2CT_x MXene is crucial. Figure 3 depicts a schematic of Nb_2CT_x MXene etching and delamination.

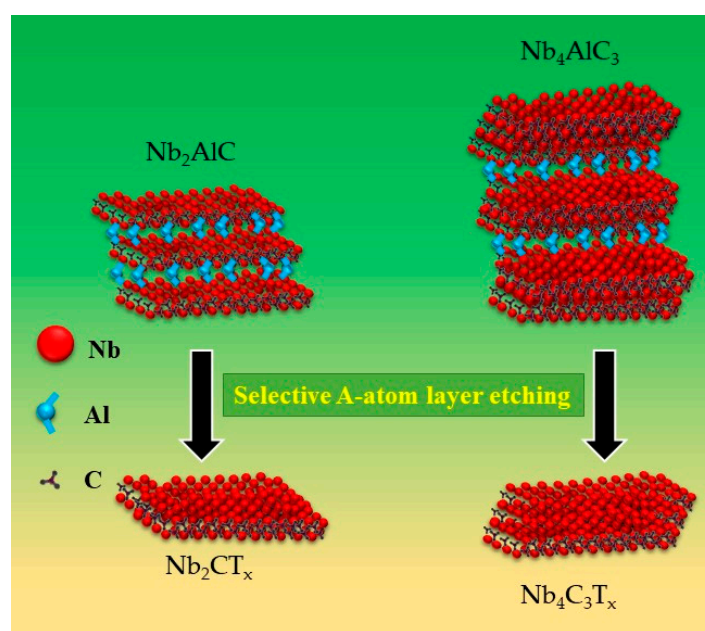


Figure 3. Schematic illustration of HF synthesis of MXene from their MAX precursor and its effects, as well as various forms of Nb_2CT_x and $Nb_4C_3T_x$ MXenes.

Table 1. Using direct HF, several etching techniques were used to create Nb₂CT_x and Nb₄C₃T_x MXenes.

MAX	MXene	HF Acid	References
Nb ₂ AlC	Nb ₂ CT _x films	50%	[28]
Nb ₄ AlC ₃	Nb ₄ C ₃ T _x flake	48–51%	[29]
Nb ₂ AlC	Nb ₂ CT _x flakes	50%	[30]
Nb ₂ AlC	Nb ₂ CT _x sheet	50%	[31]
Nb ₄ AlC ₃	Nb ₄ C ₃ T _x layer	49%	[32]
Nb ₂ AlC	Nb ₂ CT _x few-layer	40%	[33]
Nb ₄ AlC ₃	Nb ₄ C ₃ T _x film	49%	[34]
Nb ₂ AlC	Nb ₂ CT _x nanosheets	40%	[35]
Nb ₂ AlC	Nb ₂ CT _x multi-layer	49%	[36]

2.2. Molten Salt Method

A growing substitute for producing a variety of non-oxide powders is molten salt. It is a variation of powder metallurgy where the reactants are combined with salts with low melting points. When the liquid salt melts, it creates a useful medium for promoting the uniform diffusion and dissolution of the reagents, resulting in high purity with lower reaction temperature [36,37]. The usage of ball milling as a pre-treatment is also dropped when using the molten salt technique. Metal carbonates, metal fluorides, metal nitrates, and metal chlorides are a few examples of extensively utilized molten salts. Dong et al. describe the synthesis of Nb₂CT_x MXene through Lewis acidic etching in molten salts (CuCl₂/NaCl/KCl combination) heated to various temperatures for the etching process, where CuCl₂ was utilized as an etchant and the NaCl/KCl mixture as a stabilizing salt layer [38].

2.3. Other Methods

Zhou et al. synthesized the MXene ZnO/Nb₂C by the electrostatic self-assembly route [24]. A novel 2D CdS/2D Nb₂CT_x composite was synthesized by a mixture of electrostatic self-assembly using diethylene triamine (DETA) and a solvothermal reaction by Huang et al. [39–41]. Huang et al. reported that cobalt-dispersed N-doped CNTs are supported in Nb₂CT_x MXenes through the pyrolysis process [42]. The mechanochemical synthesis of Pt/Nb₂CT_x MXene composites was studied by Fan et al. [43]. Furthermore, the recent research progress on the fabrication of MXene structures was reported by Wu et al. on MXene/Xanthan Gum Hybrid Inks for Screen-Printing Electromagnetic Shielding, Joule Heater, and Piezoresistive Sensor [44]. Wang et al. developed an Nb₂CT_x/PANI-based NH₃ sensor that exhibits a superior sensitivity (2.87% ppm⁻¹) toward a wide sensing range of 1–100 ppm NH₃ and is directly driven by a facile TENG [45,46].

2.4. Synthesis Summary

Until now, only top-down approaches as mentioned above are used to synthesize the Nb₂CT_x and based MXenes. Bottom-up approaches, such as chemical vapor deposition (CVD) and atomic layer deposition (ALD), have yet to be reported due to high pollution, time-consuming procedures, low yields even in a high-cost laboratory, poor stability, and poor quality. As a result, research is needed to develop cost-effective and scalable preparation methods for high-quality MXs. To achieve these goals, eco-friendly etchants and abundantly available affordable raw materials should be prioritized. Time of production and yield are other important considerations; hence, there is a need to focus on simple and quick approaches for greater yields.

3. Properties of MXenes

MXenes' unique and useful features include conductivity, flexibility, thermal stability and so on. Figure 4 shows a diagram illustrating the creation, characteristics, and applications of MXenes.

3.1. Mechanical Properties

MXenes' mechanical characteristics must be understood and fully explored for them to be used effectively in virtually all applications. According to a previous simulation study, two-dimensional components, such as CdS_2 and elastic parameters, need to be twice as big as MAX systems [47]. The strength between A–X bonds can be measured using the bond stiffness, which is produced from the bond energy and the A–X bond length. Theoretical mechanical characteristics, such as Young's modulus, can be calculated using bond stiffness [48]. The quantity of atomic layers of MXene, indicated by the letter n in its chemical formula A_{n+1}X_n , also affects its mechanical properties.

AFM nanoindentation was used by Lipatov et al. [49] to examine the mechanical behaviors of monolayer $\text{Nb}_4\text{C}_3\text{T}_x$ membranes. They determined the $\text{Nb}_4\text{C}_3\text{T}_x$ monolayer's effective Young's modulus of 386 ± 13 GPa and its breaking strength of 26.1 ± 1.6 GPa. Comparing the $\text{Nb}_4\text{C}_3\text{T}_x$ monolayer to other 2D materials, such as reduced graphene oxide (rGO), GO, and $\text{Ti}_3\text{C}_2\text{T}_x$ material, the nanoindentation measurements Young's modulus estimate of this material is the highest [50]. This finding indicates that $\text{Nb}_4\text{C}_3\text{T}_x$ has the potential to be used in textiles, membranes, protective coatings, and other structural composite applications.

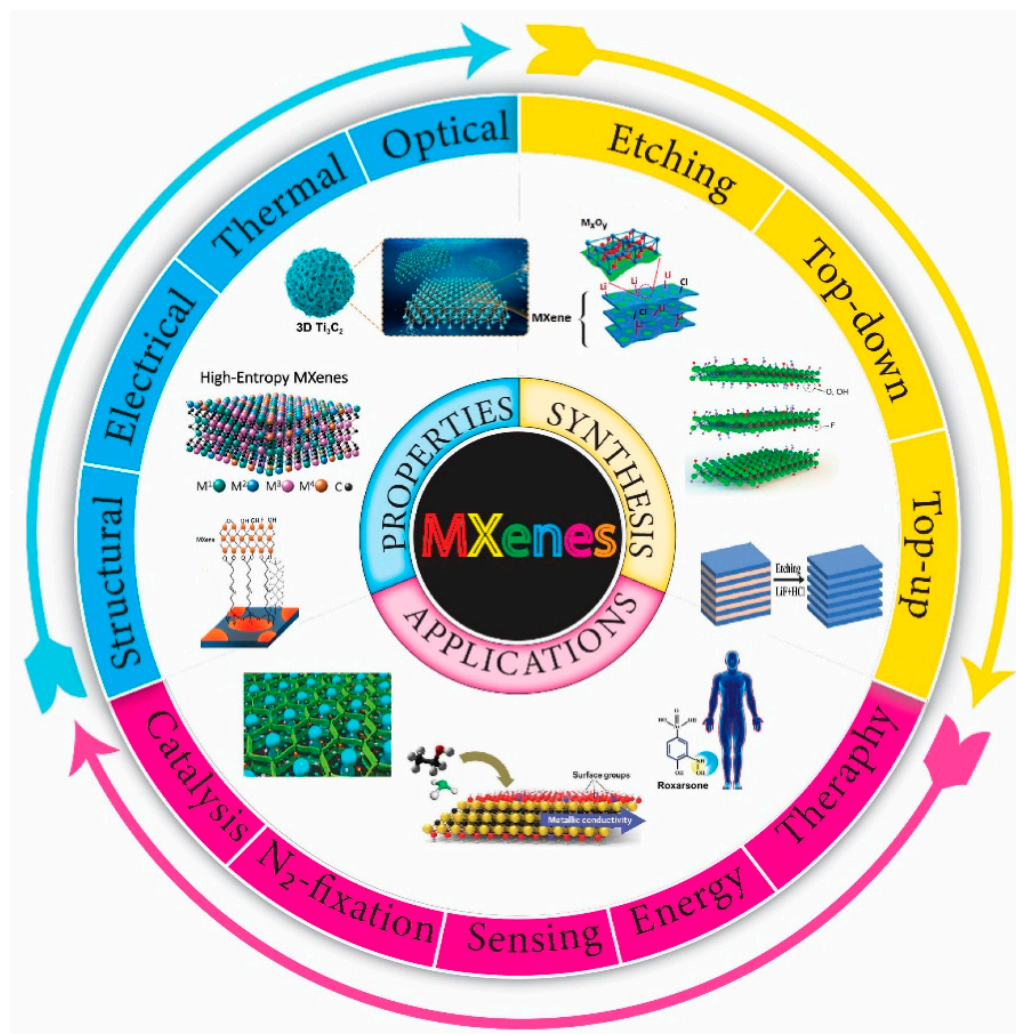


Figure 4. Diagram showing the synthesis, characteristics, and uses of MXenes. Reprinted with permission from Ref. [50].

3.2. Magnetic Property

While numerous 2D materials have been developed, the majority of them lack magnetic properties, which restricts their use in spintronics. Therefore, it has long been a top priority to produce controlled magnetism in 2D materials [51]. In forecasting the magnetic behaviors of MXenes, surface stretches are important [52]. Other explanations for the magnetic behaviors of MXenes include a rise in the density of electrons close to the Fermi region, which is explained by the *d*-group orbitals assigned to transition metal elements, or by external in-plane stretch, which is sufficient to explain potential covalent links such as *M–A* and *M–M* bonds. More investigation is required into the magnetic characteristics of MXenes. It was discovered that the superconductivity of niobium carbide MXenes is controlled by the existence of functional groups [53]. In 2D Nb₂CT_x MXene, Babar et al. [54] discovered an unusual magnetic Meissner effect, showing a superconducting material with an initial transition temperature of 12.5 K. The presence of diamagnetism and superconducting qualities were further confirmed using density functional theory (DFT) calculations, which revealed a negative magnetic moment for Nb₂CT_x [55].

3.3. Conductivity

One of the MXene's most notable properties is its electrical conductivity, which is the greatest of any synthetic 2D materials and almost 10 times stronger than that rGO [56,57]. More specifically, by adjusting extrinsic factors, such as the synthesis procedure, ultrasonication, post-etching condition, surface chemistry, and storage environment, the electrical conductivity of MXenes may be changed from $1\text{--}1.5 \times 10^4 \text{ Scm}^{-1}$ [58]. Understanding the relations between the elements and electronic properties is crucial to produce MXene materials with good conductivity.

Nb₄C₃T_x, a multilayered niobium MXene, displayed lower resistivity than Nb₂CT_x among the niobium MXenes. As a result of the additional NbC layers compared to Nb₂CT_x, this result may be explained by the greater *n* value and the existence of more MAX characters. It was discovered that Nb₄C₃T_x possesses electrical conductivity that is over 100 times greater than Nb₂CT_x. A single layer of Nb₄C₃T_x flakes exhibits electrical conductivity of $1024 \text{ G } 165 \text{ Scm}^{-1}$, which is two times greater than that of bulk Nb₄C₃T_x assemblies [59]. Ti₃C₂T_x MXene was found to have an electrical conductivity of 850 Scm^{-1} , which increased to 2410 S cm^{-1} after being calcined at 600 °C, a three-fold increase over the untreated MXene. When Ti₃C₂T_x was calcined at 400 °C, its conductivity increased by approximately 70% compared to when the sample was not calcined. Similar to this, Nb₄C₃T_x's electrical conductivity can be improved chemically. The high breakdown current density of Nb₄C₃T_x, which is comparable to that of Ti₃C₂T_x and graphene at $1.13 \times 10^8 \text{ A}\cdot\text{cm}^2$, has also been observed. Due to Nb₄C₃T_x's high breakdown current densities, additional niobium MXene members may also have high breakdown current densities, making them suitable for use in high-current applications [60].

3.4. Oxidizable Fraction Properties

The short lifespan and broad applicability of MXenes are substantially impacted by their poor oxidative stability. It is anticipated that Nb-based MXenes will be much more stable than Ti-based MXenes. The ratio between Nb and O of Nb₂CT_z MXenes has been demonstrated to decline over time, supporting the idea that Nb₂CT_z oxidizes over time. Higher “*n*” MXenes are additionally oxidatively stable, according to research on the oxidative stability of MXenes in aqueous dispersions [61]. In terms of the oxidative stability of Nb₂CT_z and Nb₄C₃T_z, research by Echols et al. found that Nb₄C₃T_z consistently had a smaller oxidizable fraction than Nb₂CT_z [62]. In contrast to Nb₂CT_z, Nb₄C₃T_z has shielded inner layers, which contribute to its stability. Additionally, it was discovered that storing Nb_{*n*+1}C_{*n*}T_z MXenes at low temperatures and adding an antioxidant (such as ascorbic acid) improved their oxidative stability. Nb₄C₃T_z and Nb₂CT_z had oxidizable fractions of 0.51 and 0.62, respectively, under typical circumstances at ambient temperature without the use of an antioxidant [62]. Even when kept at ambient temperature, these oxidizable fractions

for $\text{Nb}_4\text{C}_3\text{T}_z$ and Nb_2CT_z fell to 0.14 and 0.43, respectively. At lower temperatures, the oxidizable percentage also displayed a modest decline.

3.5. Electrochemical Behavior

Nb_2CT_x MXenes is a member of the 2D family of materials with unique electrochemical properties, due to their two-dimensional layered structure which offers a wide range of potential applications, such as energy storage, supercapacitors, fuel cells, catalysis and sustainable chemistry [63]. This is one of the most investigated Nb_2CT_x MXenes due to its outstanding electrical conductivity, good corrosion resistance, and high capacitance, high operating voltage and fast charge transfer, high capacitance [64]. In addition, its high conductivity allows for efficient redox reactions and its two-dimensional properties render it highly charge reversible. Nb_2CT_x also exhibits great potentiostatic and galvanostatic behavior in aqueous solutions. Its reversible capacitance in an aqueous environment is between 0.7–2.3 F/cm³. This is due to its high electron transport capacitance properties, which allow it to quickly convey ions through redox reactions in aqueous media [65].

3.6. Superior Hydrophilicity

In particular Nb_2CT_x MXene, one of its most remarkable properties is its hydrophilic nature. It exhibits high surface area and water-repellant properties, as its layers are rich in oxygen atoms, leading to strong electrostatic interactions with water molecules. The strong hydrophilic property of Nb_2CT_x MXene makes it a promising material for energy storage, as it allows for higher energy density and faster ion migration because of the water-repellant nature of its surfaces. Additionally, its hydrophobic nature makes it a great candidate for water purification systems, as it can effectively remove heavy metals and organic substances from contaminated water sources [66].

3.7. Thermal Property

Compared with conventional two-dimensional materials, Nb_2CT_x MXenes have excellent thermal stability and thermal conductivity. Recent studies have reported on the superior thermal properties of Nb_2CT_x MXene. Studies indicated that the thermal conductivity of the material was approximately 4.5 W/mK at 1000 K and the thermal diffusivity approximately 0.22 cm²/s. This is roughly three to five orders of magnitude higher than alumina, which is commonly used for thermal management applications. Moreover, the thermal stability of MXene Nb_2CT_x was examined by exposing it to a high temperature of 1000 °C for one hour under a nitrogen atmosphere, resulting in a negligible increase in resistivity.

The Nb_2CT_x MXene has different thermal behavior depending on the thickness of the 2D layers. It has been observed that single-layer ultrathin MXene exhibits broader thermal sensitivity in comparison to the thick film of the same composition. Furthermore, the thermal properties of Nb_2CT_x were analyzed after the incorporation of several homologous elements which resulted in a decrease in thermal diffusivity by approximately one order of magnitude [67].

3.8. Optical Property

The optical property is essentially dependent on any material for the application, such as a photocatalyst. The optical absorbance and reflectance of Nb_2CT_x MXene are reduced in the visible range by the presence of terminal groups, such as -F and -OH, and are typical for dark materials. It is possible to enhance the optical characteristics of Nb_2CT_x MXene material and raise the optical absorption coefficient of Nb_2CT_x in the visible, ultraviolet, and near-infrared regions by surface-modifying MXene with transition metals, such as Co, Ni, Fe, etc., or any doping materials. For example, L.C. Makola et al. reported the introduction of Nb_2CT_x onto g-C₃N₄, resulting in an enhanced absorption [68].

4. Applications of Nb₂CT_x MXene

4.1. In Gas Sensors

The Nb₂CT_x MXene has a high surface area and plenty of surface functional groups, which make it a good candidate for gas sensor applications. The main limitation of MXenes is atmospheric instability. Nitrogen dioxide (NO₂) is a toxic, combustible, colorless gas emitted by industrial processes and automobile emissions that depletes the ozone layer and causes acid rain. In 2022, Kumara and Pal reported the (3-aminopropyl) triethoxysilane, functionalized Nb₂CT_x for selective NO₂ gas detector [17]. The Nb₂CT_{x-0.2} APTES MXene sensor had improved sensing performance (B2.5 times that of the original Nb₂CT_x MXene sensor), as well as stability and good sensitivity ($R^2 = 0.9974$) (more than 45 days). The gas contact between the self-assembled monolayers as the result of an explicit reaction between the NO₂ gas molecule and the amine group of APTES is shown in Figure 5. To create a new equilibrium and widen the charge depletion zone, the electron transfer from APTES to NO₂ is balanced by the electron transfer from Nb₂CT_x MXene. Figure 5 shows the Nb₂CT_{x-0.2} APTES MXene's NO₂ gas sensing method [69]. The charge depletion zone can be further increased by adding NO₂ gas up to the saturation point. When the NO₂ gas is removed, the conductivity rises, and the depletion zone returns to its dry air condition. Because of the pre-stored electrons in APTES and the unusual interaction between APTES and NO₂, a low detection limit may be attainable. When NO₂ (an oxidizing gas) is introduced into the testing chamber, it catches the O₂ ions and causes many holes to form in MXene. As a result of the impediment effect, the sensor's conductivity is reduced. The sensing mechanism is described in the following equations:

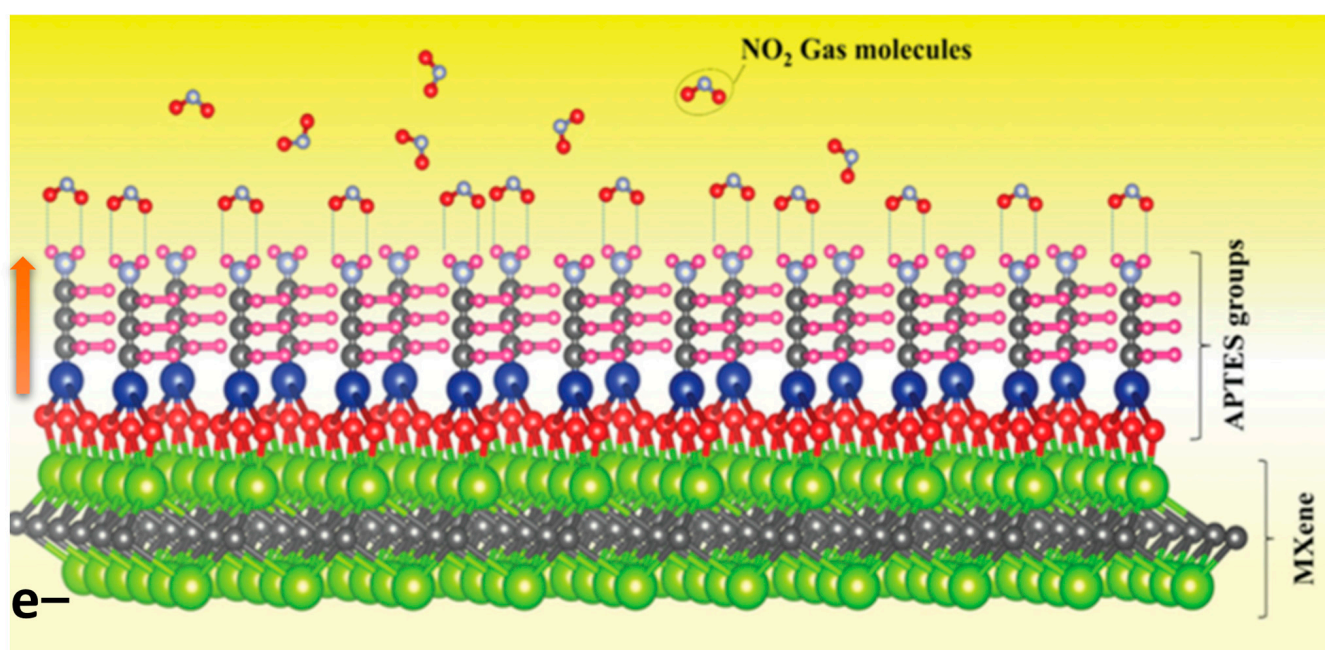
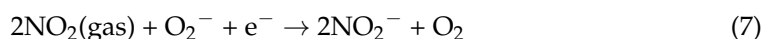
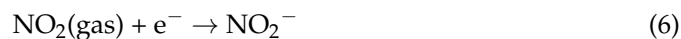


Figure 5. Sensing mechanism of Nb₂CT_{x-0.2} APTES MXene for NO₂ gas. Reprinted with permission from Ref. [70].

4.2. Supercapacitor Applications

MXenes and MXene-based materials have more volumetric capacitance than carbon-based materials, such as organic electrolytes, carbons, graphene gel sheets in water, and activated graphene [71]. Because of their increased stability and superior charging/discharging potential, $Ti_3C_2T_x$ -based materials have sparked considerable interest in supercapacitor applications [70,72]. Furthermore, the electrical conductivity of MXenes is substantially reliant on the number of atomic layers in each f.u. with consistent functional groups [73].

For example, in 2022, Zaheer et al. prepared pristine Nb_2CT_x MXene using a wet chemical etching method and coated it on Ni-foam; it displayed a specific capacitance of 258.6 F/g at poly-vinyl alcohol– H_2SO_4 electrolyte. On the other hand, they also synthesized Ni-doped Nb_2CT_x MXene, which displayed an outstanding capacitance of 666.67 F/g at 5 mV/s in the same electrolyte [74]. The cyclic stability of Ni– Nb_2CT_x MXene indicated that it could resist 10,000 cycles with an 81% capacitance retention. It had good conductivity and allowed for faster and simpler surface redox reactions that resulted in pseudo-capacitance. The electrochemical performance of virgin and Ni– Nb_2CT_x MXenes is shown in Figure 6a–d utilizing a Ni-foam (NF) electrode as the working electrode in a three-electrode assembly.

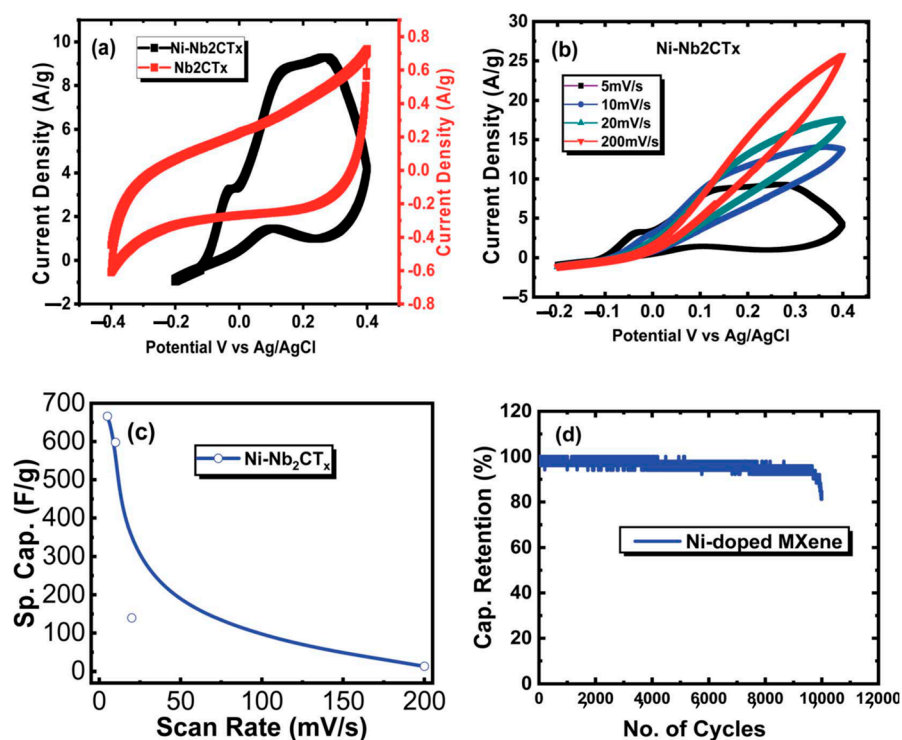


Figure 6. (a) Cyclic voltammogram (CV) curves for Nb_2CT_x and Ni– Nb_2CT_x in 1 M PVA– H_2SO_4 at 5 mV/s. (b) CV curves explicitly for Ni– Nb_2CT_x at different scan rates. (c) SC vs. scan rate for Ni– Nb_2CT_x . (d) Capacitance retention vs. cycle number for Ni– Nb_2CT_x . Reprinted with permission from Ref. [74].

In contrast, Xiao et al. reported Nb_2CT_x utilizing lithium fluoride and hydrochloric acid etchant. Meanwhile, the electrochemical performance of an Nb_2CT_x supercapacitor in an aqueous 1 M H_2SO_4 electrolyte was increased by adding multi-walled carbon nanotubes (MWCNT) as a conductive agent, yielding 202 F/g at 2 mV/s compared to 186 F/g– Nb_2CT_x . Under high mass loading, the asymmetric supercapacitor was also built using Nb_2CT_x /CNT as the negative electrode and activated carbon as the positive electrode, and it can provide a high energy density of 154.1 mWh/cm² and a maximum power density of 74,843.1 mW/cm² [75].

4.3. Battery Applications

Batteries are cutting-edge energy storage technologies that are used in industry because of their increased energy densities and superior cycle stability. Commercial batteries contain a graphite anode and a storage capacity of up to 330 mAhg^{-1} [76]. However, the limited capacity of their carbon anodes poses a challenge to the growing need for energy storage. As a result, several composites have been tested as anodes to boost their storage capacity [77]. Metals that are less expensive and more plentiful than lithium, on the other hand, have been studied in the literature [78]. Because of their lower ion diffusion barrier and better gravimetric capacity, Nb_2CT_x and related composites are regarded as promising materials for batteries. Ions of various sizes, including Li^+ , Na^+ , K^+ , Mg^{2+} , and Al^{3+} , may be injected between the Nb_2CT_x layers, making it a viable material for both lithium ion-batteries (LIBs) and non-LIBs [79]. The following work has been chosen to highlight the capacity of LIBs and other metal-ion batteries. Table 2 summarizes the Nb_2CT_x and based materials for battery applications.

Table 2. Summary of the Nb_2CT_x and based materials for battery applications.

Sl.No.	Nb_2CT_x for Battery Applications			
		Aluminum Batteries	Sodium-Ion Batteries	Li-Sulfur Batteries
1	Properties	safer and less expensive	operate at room temperature	quite expensive
2	Specific capacities	Nb_2CT_x -108 Ah/g at 0.2 A/g	$\text{Nb}_2\text{CT}_x@MoS_2@C$ -403 mA h/g at 1.0 A/g	MoS_2/Nb_2C -919.2 mAh/g, Nb_2CT_x MXene 330 mAh/g at 0.05 A/g
3	References	Li et al. [80]	Yuan et al. [81]	Zong et al. [82], Dong et al. [83]

4.3.1. Aluminum Batteries

Aluminum-ion batteries have sparked considerable attention as a potentially safer and less expensive alternative to traditional lithium-ion batteries, with quicker charging times and denser storage capacity. Nonetheless, advancement in this sector is impeded by the scarcity of appropriate cathode materials capable of supporting the reversible intercalation of $\text{Al}^{3+}/[\text{AlCl}_4]$ ions, particularly after extended cycles. Figure 7 shows the schematically Nb_2CT_x MXene-based Al battery concept [80].

Li et al. reported that Nb_2CT_x MXene cathode materials were combined with an Al anode, $\text{AlCl}_3/[\text{EMIm}]\text{Cl}$ electrolyte, and Whatman GF/C microporous membrane separators to create a Swagelok-type aluminum-ion battery [80]. After 500 cycles, the calcined Nb_2CT_x MXene cathode produced specific capacities of 108 and 80 mAh/g at charge/discharge rates of 0.2 and 0.5 A/g, respectively. Notably, following calcination, the cyclic lifespan of Nb_2CT_x MXene was increased from 300 to >500 times. We show that achieving Nb_2CT_x nanosheets with adjustable d-spacing has facilitated the migration of $[\text{AlCl}_4]$ and Al^{3+} ions in the MXene interlayers, resulting in improved charge storage. In addition, we discovered that the synthesis of niobium oxides and amorphous carbon following calcination improves the electrochemical performance of the Nb_2CT_x MXene electrode in Al batteries.

4.3.2. Sodium-Ion Batteries

As a new generation of energy storage devices takes the place of lithium-ion batteries, sodium-ion batteries that operate at room temperature have evolved. However, they are constrained by a dearth of anode materials with sufficient lifespan and outstanding rate capability. Yuan et al. created strong three-dimensional cross-linked structures using Nb_2CT_x MXene-framework MoS_2 nanosheets covered with carbon ($\text{Nb}_2\text{CT}_x@MoS_2@C$) to overcome this problem [81]. The $\text{Nb}_2\text{CT}_x@MoS_2@C$ anode offers exceptionally long cycling stability with a capacity of 403 mA h/g and just 0.01% deterioration per cycle

for 2000 cycles at 1.0 A/g. It also has an ultrahigh reversible capacity of 530 mA h/g at 0.1 A/g after 200 cycles. In terms of rate performance, this anode has a remarkable capacity retention rate of almost 88.4% from 0.1 to 1 A/g. Most crucially, the $\text{Nb}_2\text{CT}_x@MoS_2@C$ anode enables rapid charge and discharge at current densities of 20 or even 40 A/g, with capacities of 340 and 260 mAh/g, respectively, expanding the range of usable sodium-ion battery applications. Figure 8 shows an overview of the manufacturing of the 3D $\text{Nb}_2\text{CT}_x@MoS_2@C$ hybrid.

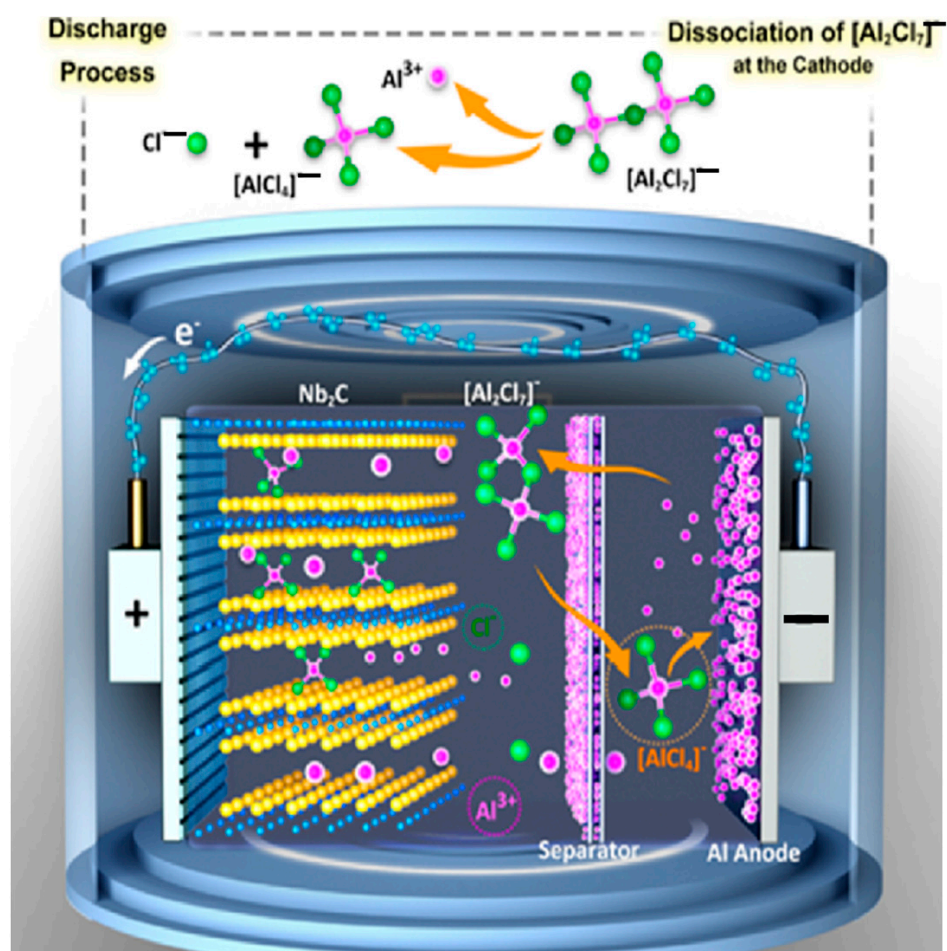


Figure 7. Nb_2CT_x MXene-based Al battery concept is described schematically. Reprinted with permission from 2022 American Chemical Society [80].

4.3.3. Li-Sulfur Batteries

Lithium-sulfur batteries (LSBs) and the hydrogen evolution reaction (HER) have a promising future for efficient catalysts created through appropriate heterostructure engineering. In this case, Nb_2C MXene was synthesized by freeze-drying and MoS_2 grew on its surface using a hydrothermal technique, as described by Zong et al. When utilized as the cathode of LSBs, the $\text{MoS}_2/\text{Nb}_2\text{C}$ hybrids demonstrated a specific capacity of 919.2 mAh/g at 0.2 °C after 200 cycles with exceptional retention of 92.2%. Figure 9 displays the fabrication of the $\text{MoS}_2/\text{Nb}_2\text{C}$ composite and its applications to the LSB's cathode and HER electrodes [82]. When employed for HER in alkaline circumstances, the $\text{MoS}_2/\text{Nb}_2\text{C}$ electrode showed remarkable long-term resilience of HER performance with a Tafel slope of 65.1 mV dec^{-1} , an overpotential of 117 mV at 10 mA cm^2 , and a Tafel slope of 65.1 mV dec^{-1} .

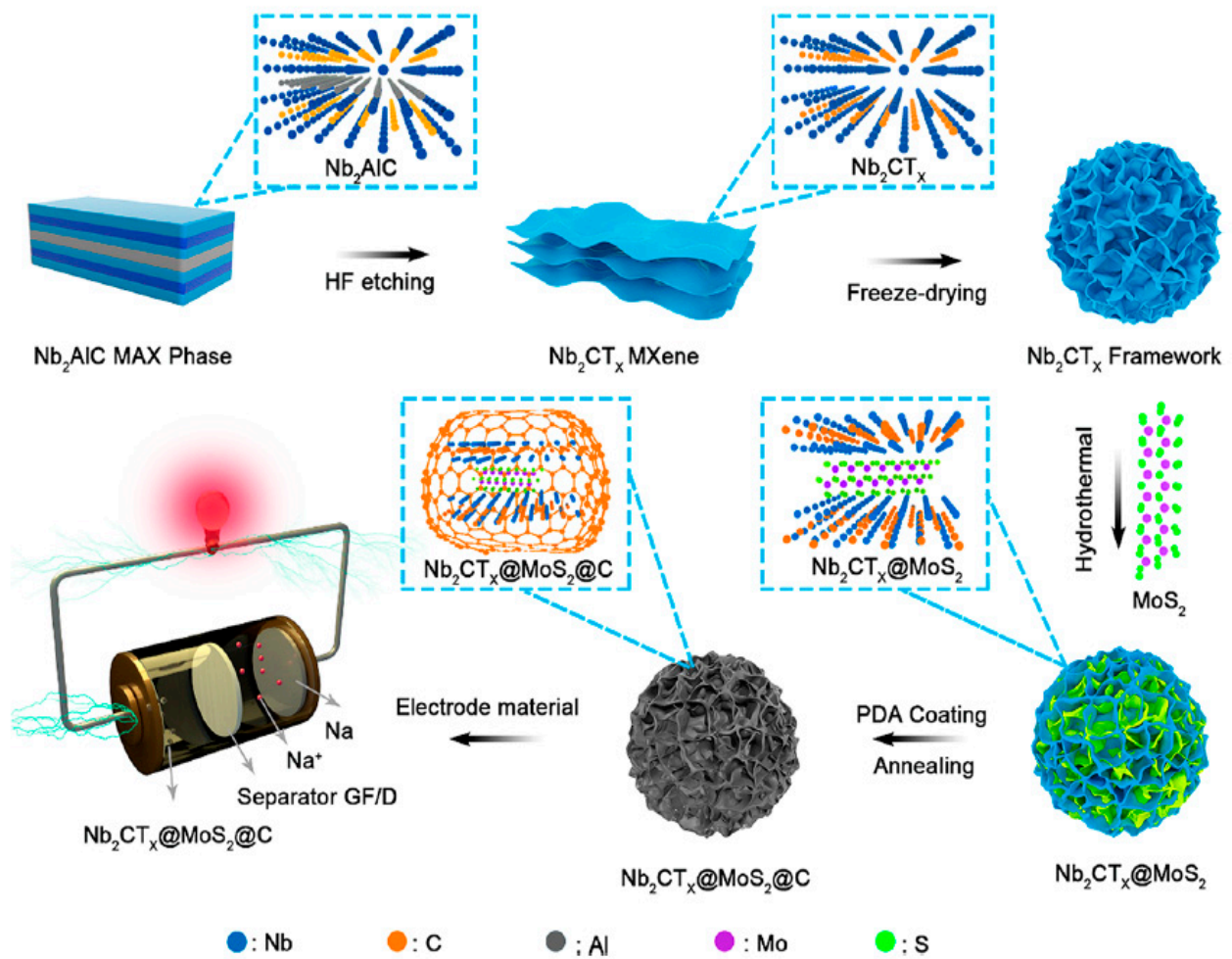


Figure 8. An overview of the manufacturing of the 3D $Nb_2CT_x@MoS_2@C$ hybrid for usage as the anode in sodium-ion batteries. Reprinted with permission from Ref. [81].

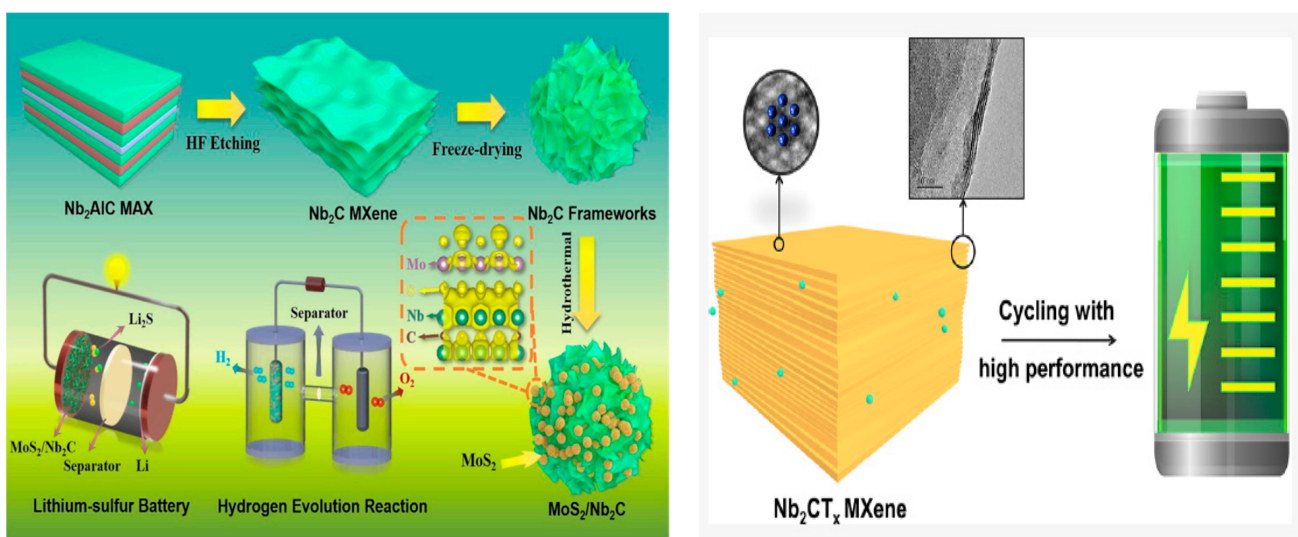


Figure 9. Diagrammatic representation of the fabrication of the MoS_2/Nb_2C composite and its applications to the LSB's cathode and HER electrodes. Reprinted with permission from Ref. [82].

As of recently, a general Lewis acidic etching strategy for producing MXenes offers a fresh perspective on the process and exhibits improved electrochemical performance in non-aqueous electrolytes thanks to the distinctive surface functional groups produced by this technique. According to Dong et al., Nb₂CT_x MXene may offer a maximum lithium storage capacity of up to 330 mAh/g at 0.05 A/g, exceeding the Nb₂CT_x MXene-derived material's maximum capacity of 205 mAh/g [84]. It is also possible to achieve high-rate performance with a capacity of 80 mAhg⁻¹ at 10 A/g (100 °C).

An Nb₂CT_x MXene that resembles an accordion was created and tested by Zhang et al. The Nb₂CT_x MXene has outstanding electrochemical performance when combined with solid Na and K and liquid KNa alloy as anodes. Examples include strong capacity retention following huge current shocks in rate performance tests and long-term stability for more than 500 cycles. In terms of the liquid electrode's ability to limit dendrite growth, the Nb₂CT_x MXene combined with liquid KNa anode performs better than that linked with solid K.

4.4. Catalysis

Tan et al. looked at the potential of Nb₄C₃T_x as a stable catalyst in the HER. To generate Nb₄C₃T_x with the greatest lattice constant, $c = 3.165$ nm, the etching settings were optimized. This Nb₄C₃T_x displayed a substantially lower overpotential than other reported MXenes, measuring a current density of 398 mA cm⁻² at 10 mV. Additionally, Nb₄C₃T_x demonstrated enhanced cyclic and long-term stability in acidic, as well as alkaline, conditions. After 1000 cycles, the overpotential of Nb₄C₃T_x fell by 30 mV, and 50 h later, the current density dramatically increased. The CO₂ oxidation of Nb₂CT_x produced a hybrid material of Nb₂O₅/C/Nb₂C that was applied as a photocatalyst for H₂ evolution via water splitting. After mild oxidation and the creation of some amorphous carbon, Nb₂O₅ grew uniformly on Nb₂C during the oxidation process. Nb₂O₅/C/Nb₂C demonstrated the highest H₂ generation rate (7.81 mmol/h gcat) under optimal conditions, which is four times more than that of pristine Nb₂O₅. The separation of photogenerated charge carriers at the hybrid interface and the tight contact between conductive Nb₂C and Nb₂O₅ may be responsible for the improved performance of Nb₂O₅/C/Nb₂C.

Nb₂CT_x can also be used as a photothermal support for metal nanoparticles in the photothermal conversion of CO₂. Wu et al. [85] conducted extensive testing on Nb₂CT_x-supported Ni nanoparticles, and the findings indicated that they had a promising CO₂ conversion rate of 8.50 mol/h g Ni under bright illumination without external heating. The photothermal catalytic activity of MXene materials is responsible for the increased CO₂ conversion rate. From the discussion above, it can be inferred that Nb₂CT_x and Nb₄C₃T_x have excellent potential for applications in Zn²⁺ ion batteries, LIBs, Li⁺ ion capacitors, Na⁺ ion batteries, photothermal catalysts, and HER catalysis because of their enhanced energy density, high volumetric capacitance, and high areal capacity. They also have outstanding reversible specific capacities with cycling stability.

Hybrid materials based on Nb₂CT_x have been used to degrade organic contaminants by photocatalysis. Methylene blue (MB), C₂₂H₂₅C₁N₂O₈ and rhodamine B (RhB) were all degraded by Cui et al. using the UV-driven photocatalytic behavior of Bi₂WO₆/Nb₂CT_x MXene hybrid nanosheets (TC-HCl) [86]. Nb₂CT_x nanosheets greatly enhance the photocatalytic activity of Bi₂WO₆ and the separation efficiency of the photogenerated carriers in this 2D/2D hybrid. In comparison to pure Bi₂WO₆, the Bi₂WO₆/Nb₂CT_x hybrid nanosheets effectively destroyed 83.1% of TC-HCl, 92.7% of MB, and 99.8% of RhB. The photodegradation rate constants for RhB and MB for the hybrid nanosheets of Bi₂WO₆/Nb₂CT_x (2 wt%) were 0.072 and 0.0285 min⁻¹. These photodegradation rate constants were 2.8 and 2.0 times greater than those of Bi₂WO₆ that had not been treated. Additionally, 0.0171 min⁻¹ was discovered to be the photodegradation rate constant of Bi₂WO₆/Nb₂CT_x (2 wt%) for TC-HCl. According to the findings of this study, Nb₂CT_x can be employed as a likely co-catalyst to improve the photodegradation efficiency of photocatalysts.

Wang et al. produced a photocatalyst based on $\text{Nb}_2\text{O}_5/\text{Nb}_2\text{CT}_x$ heterojunction with abundant O_2 vacancy for photocatalytic nitric oxide (NO) elimination [87]. At a large relative humidity of 25–75%, they discovered that the photocatalyst had good NO removal rates. The Nb_2O_5 nanorods' (001) facet has oxygen vacancies that can essentially absorb and activate the reactant gas while improving the absorption of visible light. Additionally, the $\text{Nb}_2\text{O}_5/\text{Nb}_2\text{CT}_x$ heterojunction and oxygen vacancies can improve the separation of photogenerated carriers. By developing 1D Nb_2O_5 nanorod arrays on 2D Nb_2CT_x MXene and then photo-depositing 0D Ag particles on the Nb_2O_5 nanorods to create a 0D/1D/2D hybrid structure, another Nb_2CT_x hybrid photocatalyst was created. The hybrid underwent HER testing and displayed extremely effective photogeneration of e^-h^+ pairs [88]. It was discovered that -OH is primarily absorbed as termination groups on Nb_2CT_x , leading to a low work function of 2.7 eV. The -OH-terminated Nb_2CT_x 's low work function makes hole trapping possible, and Ag particles can act as HER sites and electron storage tanks. Using methanol and glycerol as immolation agents, the ternary Ag/ Nb_2O_5 @ Nb_2CT_x nano hybrids demonstrated record HER activity of 682.2 and 824.2 mmol/g/h. When compared to other niobium-based photocatalysts, the obtained HER activity is significantly higher.

4.5. Biomedical Applications

Different biomedical applications can make use of Nb_2CT_x nanosheets in the NIR-II bio-window due to their biocompatibility, biodegradability, and unique photonic response. Nb_2CT_x was employed by Yin et al. to effectively destroy osteosarcoma (bone cancer) cells by utilizing its unique photonic response in the NIR-II bio-window, which offers high tissue penetration depth [89]. Additionally, they added Nb_2CT_x nanosheets to the 3D-printed bone mimicry scaffolds (NBGS) for the treatment of osteosarcoma. Figure 10 illustrates a schematic of the method used by NBGS for the photothermal ablation of osteosarcoma and bone regeneration.

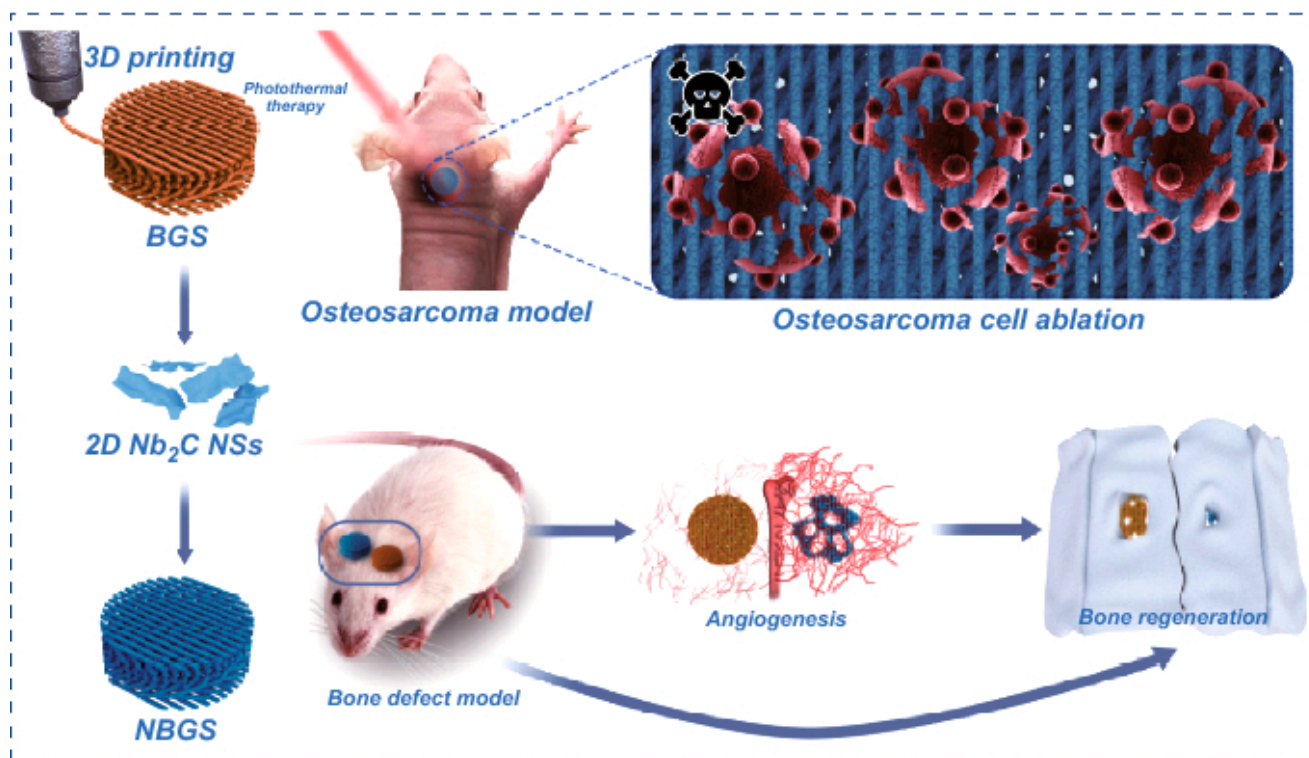


Figure 10. Process flow diagram for NBGS's photothermal osteosarcoma ablation and bone regeneration. It is possible to encourage arterialization to improve osseous repair. Reprinted with permission from Ref. [83].

Nb-created species generated by the biodegradation of Nb₂CT_x during osteosarcoma treatment encouraged blood vessel neogenesis and migration at the site of the defect. By moving more vitamins, oxygen, and immune cells past the areas of bone defects, this mechanism hastens the breakdown of NBGS. Additionally, the breakdown of NBGS creates adequate room for bone reconstruction and encourages the mineralization of new bone tissue by circulating Ca and phosphate. It was concluded that tailored Nb₂CT_x nanosheets' inherent multifunctionality makes it conceivable to employ them as a distinguishing implanted biomaterial for the efficient treatment of bone cancers.

MXenes can spontaneously absorb a large amount of reactive oxygen species (ROS) and are similarly biocompatible with other carbon-based materials. Niobium MXene's few-layered nanosheets have been used in cancer therapy and osteolytic bone disease treatment due to their capacity to absorb ROS [83]. Sun et al. used DFT calculations to assess Nb₂CT_x's capacity to absorb ROS and discovered that it had excellent ROS removal in vitro while also inhibiting the generation of inflammatory cytokines and osteoclastogenesis [83,84]. An ultra-high-molecular-weight polyethylene (UHMWPE) particle-induced osteolysis simulation has been utilized to experimentally assess ROS's capacity for absorption. The results demonstrated that Nb₂CT_x injection decreased osteolytic bone resorption on the surface of mouse calvaria. They proposed using Nb₂CT_x to stop osteolysis and other bone conditions with excessive osteoclastogenesis. In a different study, the very negative surface charges of Nb₂CT_x and Nb₄C₃T_x were changed to extremely positive values using poly-L-lysine (PLL), and the effects on ROS scavenging, cancer cell cycle arrest, and cell targeting were assessed. Both Nb₂CT_x and Nb₄C₃T_x can be utilized as ROS scavengers, and Nb₄C₃T_x was found to be more hazardous to malignant melanoma cells than Nb₂CT_x [86]. The study also revealed that PLL-modified MXene may be used to specifically target cancer cells, stop the cell cycle, and cause apoptosis (programmed cell death).

To scavenge free radicals and act as a radioprotective agent against ionizing radiation, Ren et al. explored the use of Nb₂CT_x MXene. In order to scavenge ROS such as H₂O₂, -OH radicals, and O₂ radicals, the 2D Nb₂CT_x MXene displayed antioxidant characteristics. They discovered that Nb₂CT_x (Nb₂CT_x-PVP) nanosheets functionalized with polyvinylpyrrolidone (PVP) greatly boosted in vitro cell survival by lowering radiation-induced ROS generation. Additionally, by boosting superoxide dismutase (SOD) activities and lowering malondialdehyde levels, Nb₂CT_x-PVP decreases radiation-induced pathological damage in numerous organs and restores destruction to the hematological structure in irradiated mice. The benefit of employing Nb₂CT_x-PVP is that it leaves the mouse body after a specific amount of time passes without showing any signs of toxicity.

Reding et al. examined the interactions between intestinal stem cells and MXenes for the diagnosis of gastrointestinal disorders (GI). Here, the protective and growth-inhibitory effects of Nb₂CT_x nanosheets in intestinal organoids were examined. Mice were used to isolate intestinal stem cells, which were then cultivated in organoids that replicated the genuine workings of the digestive system. The outcomes demonstrated that the right amount of nanosheets can stimulate intestinal cells without having any negative side effects. However, the growth of the organoids can be hampered by a higher nanosheet content. Additionally, as indicated in Figure 8 in the live/dead fluorescence imaging, Nb₂CT_x nanosheets demonstrated better vitality under infrared illumination in comparison to control organoids without nanosheets. This work demonstrates the significant benefits of administering Nb₂CT_x nanosheets at low concentrations to intestinal methods for maintaining and promoting cell viability during various treatment phases.

Through effective surface engineering, Nb₂CT_x has been used to alter MXene for photothermal cancer therapy. By adding a self-assembling mesopore-forming chemical (cetane-cyltrimethylammonium chloride [CTAC]) and altering it with mesoporous SiO₂, Han et al. created a unique “therapeutic mesopore” layer on the surface of Nb₂CT_x. For targeted tumor enhancement, the material underwent PEGylation (conjugation with polyethylene glycol [PEG]) and conjugation with cyclic arginine-glycine-aspartic acid pentapeptide (cRGDyC) [87]. With a high drug loading capacity of approximately 33%, the use of CTAC in mesopores facilitates chemo drug loading, and surface modification with cRGDyC specifically detects integrin overexpressed on the membrane of cancer cells. Under laser irradiation in the NIR-II bio-window (1064 nm), the Nb₂CT_x core causes a high photothermal conversion capacity (28.6%), resulting in improved photothermal hyperthermia. With an inhibitory efficiency of 92.37%, the Nb₂CT_x mesopore displayed targeted and improved chemotherapy and generated photothermal hyperthermia in the cancer cell line and the associated tumor xenograft [88]. This paper presents an effective method for surface engineering of 2D MXenes for diverse biological uses in photothermal therapy and chemotherapy, among other enhanced cancer therapies. Figure 11 shows the evaluation of the tissue penetration depth for NIR-I and NIR-II photothermal conversion *in vitro* and *in vivo*.

The highly successful *in vivo* photothermal ablation of tumor xenografts using Nb₂CT_x-PVP nanosheets was demonstrated in a different study using NIR-I and NIR-II bio-windows [89].

In vitro and *in vivo* tests of the Nb₂CT_x-PVP nanosheets revealed outstanding biocompatibility and physiological stability with no obvious toxicity. The ability of an MXene-based nanotherapeutic agent for safe *in vivo* use was also proven, with the possibility of enzymatic biodegradation of the Nb₂CT_x-PVP nanosheets using human myeloperoxidase. This viewpoint led to an evaluation of Nb₂CT_x-PVP nanosheets’ *in vivo* photothermal ablation versus tumor xenografts. The photothermal conversion efficiency of these ultrathin, laterally nanosized Nb₂CT_x-PVP nanosheets—36.4% at NIR-I and 45.65% at NIR-II—showed encouraging photothermal stability. After 10 min of exposure to NIR-I and NIR-II lasers, respectively, the tumor site temperatures improved from 30 °C to 61 °C and from 30 °C to 65 °C after the injection of Nb₂CT_x-PVP nanosheets into mice. Figure 12 depicts a comparable thermal picture. Figure 13 images of 4T1 tumor-bearing mice and their tumor locations after 16 days of treatment demonstrate total eradication of the tumor. Figure 13 also includes various staining images demonstrating pathological alterations in the tumor tissues. When compared to the other circumstances evaluated, the Nb₂CT_x-PVP + NIR-I and Nb₂C-PVP + NIR-II groups exhibit highly substantial tumor cell necrosis when stained with H&E and TUNEL (terminal deoxynucleotidyl transferase dUTP nick end labeling). For the Nb₂CT_x-PVP + NIR-I and Nb₂CT_x-PVP + NIR-II groups, Ki-67 antibody staining revealed a marked inhibitory effect on cell growth. Figure 12 shows the 2D Biodegradable Nb₂C (modified with PVP) Schematic Illustration for *In Vivo* Photothermal Tumor Ablation in NIR-I and NIR-II Bio windows.

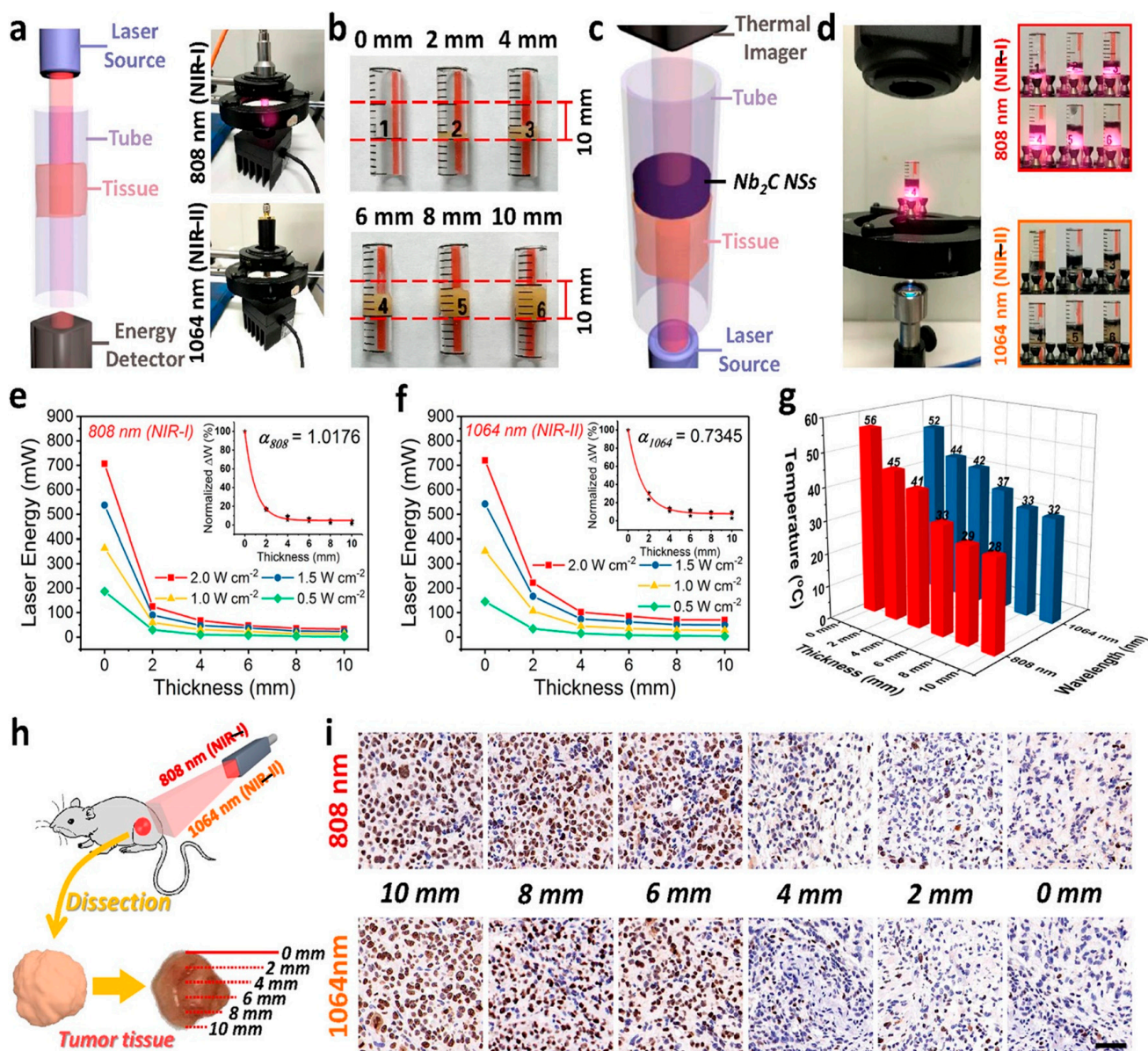


Figure 11. Evaluation of the tissue penetration depth for NIR-I and NIR-II photothermal conversion in vitro and in vivo. (a) A schematic diagram and the tools needed to measure the NIR laser's capacity to penetrate tissue at 808 and 1064 nm. (b) Chicken breast tissues are attached in clear tubing in varying thicknesses (0, 2, 4, 6, 8, and 10 mm). (c) A schematic diagram and (d) the tools needed for the tissue-penetrating NIR laser (1.0 W cm^{-2} , 80 g mL^{-1}) to demonstrate photothermal conversion of aqueous solutions of distributed $\text{Nb}_2\text{C NSs}$. (e) NIR-I laser energy intensities (808 nm) entering tissues at various thicknesses. Inset: Normalized NIR-I radiation passing through tissues at various depths. 808: the NIR-I laser's attenuation coefficient at 808 nm. (f) NIR-II laser energy intensities (1064 nm) pass through various tissue thicknesses. Inset: Normalized NIR-II energy permeating various depths of tissue. 1064: the NIR-II laser's attenuation coefficient at 1064. (g) Photothermal conversion causes the temperature of aqueous solutions of dispersed $\text{Nb}_2\text{C NSs}$ to rise when they are exposed to tissue-penetrating NIR-I and NIR-II lasers. (h) Schematic representation of in vivo tumor tissue penetration using NIR-I and NIR-II for photothermal conversion. (i) Antigen Ki-67 immunofluorescence staining for cellular proliferation in dissected tumor tissues at various depths (0, 2, 4, 6, 8, and 10 mm). The scale bar across all photographs is 50 μm . Reprinted with permission from Ref. [90].

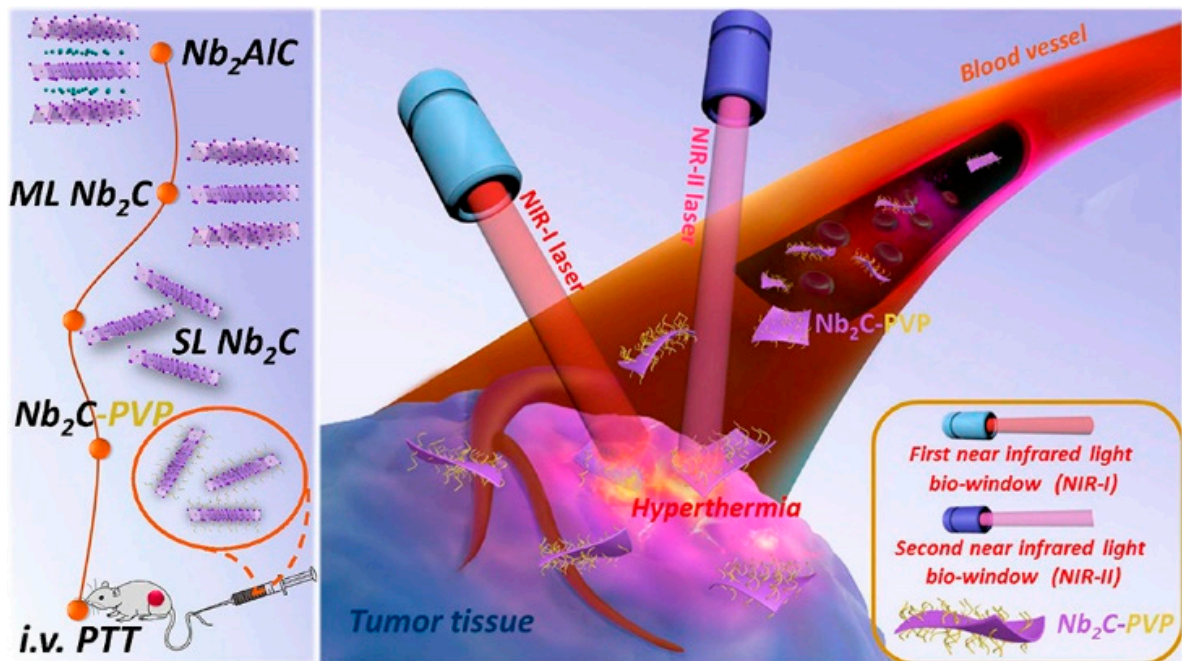


Figure 12. 2D biodegradable Nb₂C (modified with PVP) schematic illustration for in vivo photothermal tumor ablation in NIR-I and NIR-II bio-windows. Reprinted with permission from Ref. [90].



Figure 13. Photographs of 4T1 tumor-bearing mice after the control and different treatments in 16 days' period. Reprinted with permission from Ref. [90].

Medical implants have employed niobium carbide MXene to perform a variety of multimodal tasks, including bacterial infection eradication and tissue regeneration. Nb₂CT_x MXene has been added to titanium plate-based implants (Nb₂CT_x @TP) to enable the direct dissolution of biofilms and bacterial eradication [91]. As a result of their capacity to sensitize microorganisms through photothermal transduction, which lowers the temperature needed to eradicate germs, these implants do not harm healthy tissue. Furthermore, by lowering pro-inflammatory responses and scavenging too many reactive oxygen types in infectious microenvironments, the medical implant Nb₂CT_x @TP encourages angiogenesis and tissue remodeling. The characteristics of Nb₂CT_x, such as its biodegradability, biocompatibility, ability to absorb ROS, antioxidant qualities for scavenging ROS, and the distinctive photonic response of Nb₂CT_x nanosheets in the NIR-II bio-window, can be used in a variety of biomedical applications.

4.6. Electromagnetic Interference (EMI) Shielding Applications

Owing to its unique layered structure, numerous inherent flaws, substantial specific surface area, and unique metallic characteristics, MXene materials have been exploited in EMI shielding applications [92]. It has been proven that Ti-based MXenes are effective in EMI shielding applications [85]. Rajavel et al. also looked at the viability of employing Nb₂CT_x for EMI shielding applications [90]. For EMI shielding applications, they combined lamellar structured Nb₂CT_x with one-step removed low-stratified Nb₂CT_x. When low-layered Nb₂CT_x and lamellar-structured Nb₂CT_x are combined, it is possible to build several electrically conductive channels that have a higher capacity to absorb electromagnetic (EM) waves, making them suitable for EMI shielding. A composite of Nb₂CT_x and wax with an 80% Nb₂CT_x loading was created and expanded at a thickness of $t = 1$ mm over 100 h. The composite material exhibited an EMI shielding efficiency of approximately 44.09 G 1.99 dB at 12 GHz when it was employed for EMI shielding. Eddy's current losses and conduction losses provide a comprehensive explanation of the EMI attenuation mechanism. Lamellar and few-layer Nb₂CT_x nanostructures can be combined to create intriguing new shielding materials that are suitable for difficult applications. Another study created a composite of rGO, Nb₂CT_x, and Fe₃O₄ that had improved EM wave absorption capabilities, with a minimum reflection loss of 59.17 dB at 11.8 GHz and an equal absorber $t = 2.5$ mm. It was discovered that an absorber with a $t = 1.5$ to 3 mm may be modified for a frequency over 8.5 to 18 GHz with an active absorption bandwidth (EAB, reflection loss [RL]% 10 dB) of 6.8 GHz [93]. The synergistic effects of excellent impedance similar and the several loss mechanisms of rGO/Nb₂CT_x/Fe₃O₄ can be credited for the composite's increased absorption capacity.

4.7. Microwave Absorption Applications

Similarly, hybrids built on Nb₂CT_x have been investigated for use in microwave absorption. Nb₂O₅/Nb₂CT_x hybrids were quickly synthesized using a microwave-assisted hydrothermal method by Song et al. and studied their absorption capacity. Here, several Nb₂O₅ structures were produced on-site and intercalated between the Nb₂CT_x layers [94–97]. The incomplete reaction between Nb₂O₅ and Nb₂CT_x resulted in the formation of the Nb₂O₅/Nb₂CT_x hybrids. In comparison to Nb₂CT_x that had not been treated, the Nb₂O₅/Nb₂CT_x hybrids had increased microwave absorption performance by 99.99%. The enhanced lamellar spacing of Nb₂CT_x, the unique shape of Nb₂O₅, and the better impedance matching capabilities are all accountable for the enhanced performance of microwave absorption.

5. Possibilities for Commercial Applications

Nb₂CT_x's properties, such as redox activity, ion intercalation, high conductivity, surface chemistry, structural stability, and flexibility to form composites, make it a promising applicant for a variety of saleable uses, such as catalysis, power storage, antimicrobial,

sensors, and energy conversion. Nb₂CT_x is used for a diversity of purposes, including environmental, biological, electrical, aeronautical, and opto-spintronics [98].

Nb₂CT_x MXene-based materials contribute to better storage and cycling performance in batteries and supercapacitors for power storage applications. Due to their increased power density and cycle performance, lithium-ion batteries are unavoidable for electronic gadgets, electric vehicles, portable devices, and the continuous process of the electrical power grid with the integration of renewable energy resources. However, the anode-like graphite utilized in industrial applications has a limited storage capacity of 330 mAh g⁻¹, which must be enhanced to satisfy potential requirements. Beyond the storage capacity constraint, Li must be replaced with a plentiful and less expensive alternative. Nb₂CT_x MXene contributes by boosting the power density of Li-ion batteries and also by enhancing the other metal-ion batteries. According to theoretical capacities provided by Anasori et al. [91], aluminum, potassium, and sodium could be Li replacements. However, Li-ion batteries with Nb₂CT_x MXene composite electrodes have been found to exhibit unrivaled energy densities, signaling a feasible commercial application. Supercapacitors with high power densities and cycle capacity are critical for electric vehicles and power applications. Nb₂CT_x MXene-based supercapacitor electrodes perform similarly or better than off-the-shelf activated carbon-based supercapacitors. As a result, supercapacitors are a likely industrial use of Nb₂CT_x MXene-based materials. An additional possible commercial application of Nb₂CT_x MXene is its antibacterial properties, which are superior to any well-studied antimicrobial compounds, such as GO/rGO, for healing infected wounds [99]. Nb₂CT_x MXene was recently used to cure chronic drug-resistant lesions by Zhou et al. Nb₂CT_x MXene composites also demonstrated encouraging outcomes as electrocatalysts in the H₂ evolution process, adding to the global search for pure, inexpensive, and non-fossil fuels. Nb₂CT_x MXene has a potential industrial and commercial application as a gas and strain sensor [100]. Sports, air/breath assessment, health monitoring, environmental monitoring, and robotics could all benefit from this technology. Nb₂CT_x MXene-based materials have the potential to be used in industrial and commercial applications, such as sensors, drug delivery, bone regeneration, photovoltaic devices, energy storage, thermoelectric generation, bioimaging, antibacterial activity, electrocatalysis, photocatalysis, and tribology [101–133]. Nb₂CT_x MXene and its composites' qualities make them a viable option for such a diverse variety of industrial applications, contributing to the resolution of key global concerns. Environmental concerns, health problems, and a low-cost and consistent source of fuel and energy are among the challenges.

6. Conclusions and Prospects

Due to its distinct composition, properties, and sheet-like structure, Nb₂CT_x is among the most intriguing nanostructures for a wide range of applications. Nb₂CT_x has been widely used in a range of energy purposes from batteries to supercapacitors, H₂ evolution reactions, and environmental applications, such as sensing, antibacterial, and so on. Numerous efforts have recently been made to improve its recyclability, biocompatibility, and structural stability in the surrounding atmosphere to improve its functioning for environmental and energy purposes. To tackle some of the shortcomings of pure Nb₂CT_x, such as aggregation and long-term stability, a wide range of Nb₂CT_x-constructed heterojunctions, containing polymeric and metal oxide materials, and CNTs were also created. To defeat the current hurdles, more in-depth research is required for Nb₂CT_x-based MXenes to be the pioneer for environmental and energy purposes. No doubt Nb₂CT_x has become a next-generation material with enormous potential in a variety of applications. Yet, many obstacles still stand in the way of its actual practical application. The following are a few of the major challenges:

1. The traditional synthesis of Nb₂CT_x uses HF etching, which poses a protection and environmental risk, making large-scale production challenging. A possible area of research is the use of green materials and the replacement of HF with less toxic compounds in the manufacture of Nb₂CT_x. Future studies could concentrate on the production of surface terminations utilizing environmentally acceptable materials.
2. Drawing-up superior Nb₂CT_x with the appropriate properties might be a research emphasis. This is because the surface chemistry of Nb₂CT_x is sensitive to synthesis conditions. Nb₂CT_x may have a multilayered and accordion-like structure rather than 2D sheets, limiting its utility in environmental applications. To obtain flakes of Nb₂CT_x with tunable morphological features, a method should be established.
3. Another future challenge will be to produce Nb₂CT_x cheaply and with high returns. The development of inexpensive, efficient, and environmentally friendly Nb₂CT_x manufacturing on an industrial scale is required for the practical use of Nb₂CT_x. Another potential difficulty is the aggregation of Nb₂CT_x layers, which lowers the surface area, and thus, the storage capacity. Aggregation resolution can enhance the energy capacity of Nb₂CT_x-based electrodes and purifying performance for environmental purposes.
4. Future research should also concentrate on the precise prediction of Nb₂CT_x and its composites, which is challenging owing to heterogeneous surface terminations since existing approaches call for homogeneous terminations, which are still a work in progress. There is yet no technique for evenly terminating surface groups, such as fluorine, hydroxyl, oxygen, or hydrogen. Researchers must also focus on the processes at work of structural changes brought on by functional groupings.
5. Another difficulty for Nb₂CT_x and related materials is to create structures with controllable features for purposes such as energy storage. Many techniques including heterostructure, ion intercalation, and functional group control have been suggested to enhance the storage capability of Nb₂CT_x. Further research is required to better identify the energy storage process so that a combination of modifications can be scientifically preferred to obtain the best solution based on needs.
6. The expense and structural instability of Nb₂CT_x could be a barrier to industrial use. The expense is due to the use of a costly MAX precursor during the synthesis. Advanced material synthesis with lower production costs is required. Additional composites and solvents must be investigated and assessed for varied purposes to alleviate structural instability. The creation of a packaging solution is essential for extending the service life of Nb₂CT_x-based devices.
7. So far, only a few Nb₂CT_x-based MXenes have been experimentally applied to specific applications. Hence, there is a need to expand its applications to biomedical, electrodes for flexible all-solid-state supercapacitors, photothermal therapy, electronics, such as FET, for tunable band gaps, lubricant oil, biosensors, antibacterial activity, water purification, H₂ generation, O₂ evolution electrocatalyst, sensors such as for NH₃ and CO₂, nuclear waste management, nanofiltration, dye adsorption, electromagnetic interference (EMI) shielding, and more.

Author Contributions: Conceptualization, T.R. and A.-H.I.M.; methodology, T.R. and A.-H.I.M.; software, T.R.; validation, T.R. and A.-H.I.M.; formal analysis, T.R. and A.-H.I.M.; investigation, T.R.; resources, T.R.; data curation, T.R., A.-H.I.M. and M.S.A.E.; writing—original draft preparation, T.R.; writing—review and editing, T.R., A.-H.I.M. and M.S.A.E.; visualization, T.R., A.-H.I.M. and M.S.A.E.; supervision, A.-H.I.M. and M.S.A.E.; project administration, A.-H.I.M. and M.S.A.E.; funding acquisition, A.-H.I.M. and M.S.A.E. All authors have read and agreed to the published version of the manuscript.

Funding: This research was funded by the UAE University (Grant No. 31R238), and the international collaboration project of the University of California, Berkeley.

Conflicts of Interest: The authors declare no conflict of interest.

References

1. Gogotsi, Y.; Anasori, B. The Rise of MXenes. *ACS Nano* **2019**, *13*, 8491–8494. [CrossRef] [PubMed]
2. Bhimanapati, G.R.; Lin, Z.; Meunier, V.; Jung, Y.; Cha, J.; Das, S.; Xiao, D.; Son, Y.; Strano, M.S.; Cooper, V.R.; et al. Recent Advances in Two-Dimensional Materials beyond Graphene. *ACS Nano* **2015**, *9*, 11509–11539. [CrossRef] [PubMed]
3. Zhong, Y.; Xia, X.; Shi, F.; Zhan, J.; Tu, J.; Fan, H.J. Transition Metal Carbides and Nitrides in Energy Storage and Conversion. *Adv. Sci.* **2016**, *3*, 1500286. [CrossRef] [PubMed]
4. Naguib, M.; Mochalin, N.V.; Barsoum, W.M.; Gogotsi, Y. 25th anniversary article: MXenes: A new family of two-dimensional materials. *Adv. Mater.* **2014**, *26*, 992–1005. [CrossRef] [PubMed]
5. Ramachandran, T.; Mourad, A.-H.I.; Raji, R.K.; Krishnapriya, R.; Cherupurakal, N.; Subhan, A.; Al-Douri, Y. KOH mediated hydrothermally synthesized hexagonal-CoMn₂O₄ for energy storage supercapacitor applications. *Int. J. Energy Res.* **2022**, *46*, 16823–16838. [CrossRef]
6. Zhang, X.; Wang, Z.; Shao, G. Theoretical identification of layered MXene phase Na_xTi₄C₂O₄ as superb anodes for rechargeable sodium-ion batteries. *J. Mater. Chem. A Mater. Energy Sustain.* **2020**, *8*, 11177–11187. [CrossRef]
7. Long, Q.M.; Tang, K.K.; Xiao, J.; Li, J.Y.; Chen, J.; Gao, H.; Chen, H.W.; Liu, T.C.; Liu, H. Recent advances on MXene based materials for energy storage applications. *Mater. Today Sustain.* **2022**, *19*, 100163. [CrossRef]
8. Wu, Y.; Sun, Y.; Zheng, J.; Rong, J.; Li, H.; Niu, L. MXenes: Advanced materials in potassium ion batteries. *Chem. Eng. J.* **2021**, *404*, 126565. [CrossRef]
9. Nasrin, K.; Sudharshan, V.; Subramani, K.; Sathish, M. Insights into 2D/2D MXene heterostructures for improved synergy in structure toward next-generation supercapacitors: A review. *Adv. Funct. Mater.* **2022**, *32*, 2110267. [CrossRef]
10. Zhao, Q.; Jiang, Y.; Duan, Z.; Yuan, Z.; Zha, J.; Wu, Z.; Huang, Q.; Zhou, Z.; Li, H.; He, F.; et al. A Nb₂CT_x/sodium alginate-based composite film with neuron-like network for self-powered humidity sensing. *Chem. Eng. J.* **2022**, *438*, 135588. [CrossRef]
11. Zhao, W.; Cao, J.; Wang, F.; Tian, F.; Zheng, W.; Bao, Y.; Zhang, K.; Zhang, Z.; Yu, J.; Xu, J.; et al. 3D Printing of Stretchable, Adhesive and Conductive Ti₃C₂T_x-Polyacrylic Acid Hydrogels. *Polymers* **2022**, *14*, 1992. [CrossRef] [PubMed]
12. Xu, X.; Yang, L.; Zheng, W.; Zhang, H.; Wu, F.; Tian, Z.; Zhang, P.; Sun, Z.M. MXenes with applications in supercapacitors and secondary batteries: A comprehensive review. *Mater. Rep. Energy* **2022**, *2*, 100080. [CrossRef]
13. Abdul Rasheed, P.; Pandey, R.P.; Banat, F.; Hasan, S.W. Recent advances in niobium MXenes: Synthesis, properties, and emerging applications. *Matter* **2022**, *5*, 546–572. [CrossRef]
14. MXene Synthesis. Available online: <https://nano.materials.drexel.edu/max-phases-and-mxenes-synthesis/> (accessed on 5 January 2023).
15. Huang, C.; Shi, S.; Yu, H. Work Function Adjustment of Nb₂CT_x Nanoflakes as Hole and Electron Transport Layers in Organic Solar Cells by Controlling Surface Functional Groups. *ACS Energy Lett.* **2021**, *6*, 3464–3472. [CrossRef]
16. Zhu, H.; Xue, S.; Liang, Z.; Liang, X.; Li, G.; Ren, X.; Gao, L.; Li, Q.; Ma, T.; Liu, A. Self-assembly synthesis of Ni-decorated Nb₂C MXene as an efficient and stable catalyst towards electrochemical nitrogen reduction. *Ceram. Int.* **2022**, *48*, 20599–20604. [CrossRef]
17. Pandey, R.P.; Rasheed, P.A.; Gomez, T.; Rasool, K.; Ponraj, J.; Prenger, K.; Naguib, M.; Mahmoud, K.A. Effect of Sheet Size and Atomic Structure on the Antibacterial Activity of Nb-MXene Nanosheets. *ACS Appl. Nano Mater.* **2020**, *3*, 11372–11382. [CrossRef]
18. Li, J.; Zeng, F.; El-Demellawi, J.K.; Lin, Q.; Xi, S.; Wu, J.; Tang, J.; Zhang, X.; Liu, X.; Tu, S. Nb₂CT_x MXene Cathode for High-Capacity Rechargeable Aluminum Batteries with Prolonged Cycle Lifetime. *ACS Appl. Mater. Interfaces* **2022**, *14*, 45254–45262. [CrossRef]
19. Gul, S.; Serna, M.I.; Zahra, S.A.; Arif, N.; Iqbal, M.; Akinwande, D.; Rizwan, S. Un-doped and Er-adsorbed layered Nb₂C MXene for efficient hydrazine sensing application. *Surf. Interfaces* **2021**, *24*, 101074. [CrossRef]
20. Naveen Kumar, A.; Pal, K. Amine-functionalized stable Nb₂CT_x MXene toward room temperature ultrasensitive NO₂ gas sensor. *Mater. Adv.* **2022**, *3*, 5151–5162. [CrossRef]
21. Zong, H.; Hu, L.; Gong, S.; Yu, K.; Zhu, Z. Flower-petal-like Nb₂C MXene combined with MoS₂ as bifunctional catalysts towards enhanced lithium-sulfur batteries and hydrogen evolution. *Electrochim. Acta* **2022**, *404*, 139781. [CrossRef]
22. Zhang, W.; Jin, H.; Chen, G.; Zhang, J. Sandwich-like N-doped carbon nanotube@Nb₂C MXene composite for high performance alkali ion batteries. *Ceram. Int.* **2021**, *47*, 20610–20616. [CrossRef]
23. Byeon, A.; Glushenkov, A.M.; Anasori, B.; Urbankowski, P.; Li, J.; Byles, B.W.; Blake, B.; Van Aken, K.L.; Kota, S.; Pomerantseva, E.; et al. Lithium-ion capacitors with 2D Nb₂CT_x (MXene)—Carbon nanotube electrodes. *J. Power Sources* **2016**, *326*, 686–694. [CrossRef]
24. Zhou, W.; Yu, B.; Zhu, J.; Li, K.; Tian, S. Hierarchical ZnO/MXene (Nb₂C and V₂C) heterostructure with efficient electron transfer for enhanced photocatalytic activity. *Appl. Surf. Sci.* **2022**, *590*, 153095. [CrossRef]
25. Yan, Y.; Han, H.; Dai, Y.; Zhu, H.; Liu, W.; Tang, X.; Gan, W.; Li, H. Nb₂CT_x MXene Nanosheets for Dye Adsorption. *ACS Appl. Nano Mater.* **2021**, *4*, 11763–11769. [CrossRef]
26. Liu, Z.; El-Demellawi, K.J.; Bakr, M.O.; Ooi, S.B.; Alshareef, N.H. Plasmonic Nb₂CT_x MXene-MAPbI₃ Heterostructure for Self-Powered Visible-NIR Photodiodes. *ACS Nano* **2022**, *16*, 8. [CrossRef]
27. Nasrin, K.; Sudharshan, V.; Arunkumar, M.; Sathish, M. 2D/2D Nanoarchitected Nb₂C/Ti₃C₂ MXene Heterointerface for High-Energy Supercapacitors with Sustainable Life Cycle. *ACS Appl. Mater. Interfaces* **2022**, *14*, 21038–21049. [CrossRef] [PubMed]

28. Naguib, M.; Halim, J.; Lu, J.; Cook, K.M.; Hultman, L.; Gogotsi, Y.; Barsoum, M.W. New two-dimensional niobium and vanadium carbides as promising materials for Li-Ion batteries. *J. Am. Chem. Soc.* **2013**, *135*, 15966–15969. [[CrossRef](#)]
29. Ghidui, M.; Naguib, M.; Shi, C.; Mashtalir, O.; Pan, L.M.; Zhang, B.; Yang, J.; Gogotsi, Y.; Billinge, S.J.L.; Barsoum, M.W. Synthesis and characterization of twodimensional Nb₄C₃ (MXene). *Chem. Commun.* **2014**, *50*, 9517–9520. [[CrossRef](#)]
30. Mashtalir, O.; Lukatskaya, M.R.; Zhao, M.Q.; Barsoum, M.W.; Gogotsi, Y. Amine-assisted delamination of Nb₂C MXene for Li-ion energy storage devices. *Adv. Mater.* **2015**, *27*, 3501–3506. [[CrossRef](#)]
31. Lin, H.; Gao, S.; Dai, C.; Chen, Y.; Shi, J. A two-dimensional biodegradable niobium carbide (MXene) for photothermal tumor eradication in NIR-I and NIR-II biowindows. *J. Am. Chem. Soc.* **2017**, *139*, 16235–16247. [[CrossRef](#)]
32. Zhao, S.; Meng, X.; Zhu, K.; Du, F.; Chen, G.; Wei, Y.; Gogotsi, Y.; Gao, Y. Li-ion uptake and increase in interlayer spacing of Nb₄C₃ MXene. *Energy Storage Mater.* **2017**, *8*, 42–48. [[CrossRef](#)]
33. Zhao, J.; Wen, J.; Bai, L.; Xiao, J.; Zheng, R.; Shan, X.; Li, L.; Gao, H.; Zhang, X. One-step synthesis of few-layer niobium carbide MXene as a promising anode material for high-rate lithium ion batteries. *Dalton Trans.* **2019**, *48*, 14433–14439. [[CrossRef](#)] [[PubMed](#)]
34. Zhao, S.; Chen, C.; Zhao, X.; Chu, X.; Du, F.; Chen, G.; Gogotsi, Y.; Gao, Y.; Dall Agnese, Y. Flexible Nb₄C₃T_x film with large interlayer spacing for highperformance supercapacitors. *Adv. Funct. Mater.* **2020**, *30*, 2000815. [[CrossRef](#)]
35. Wang, Y.; Wang, Y.; Chen, K.; Qi, K.; Xue, T.; Zhang, H.; He, J.; Xiao, S. Niobium carbide MXenes with broad-band nonlinear optical response and ultrafast carrier dynamics. *ACS Nano* **2020**, *14*, 10492–10502. [[CrossRef](#)]
36. Yang, Z.; Gao, L.; Chen, H.; Zhang, F.; Yang, Q.; Ren, X.; Din, S.Z.U.; Li, C.; Leng, J.; Zhang, J.; et al. Broadband few-layer niobium carbide MXene as saturable absorber for solid-state lasers. *Opt. Laser Technol.* **2021**, *142*, 107199. [[CrossRef](#)]
37. Wu, Z.; Li, C.; Li, Z.; Feng, K.; Cai, M.; Zhang, D.; Wang, S.; Chu, M.; Zhang, C.; Shen, J.; et al. Niobium and titanium carbides (MXenes) as superior photothermal supports for CO₂ photocatalysis. *ACS Nano* **2021**, *15*, 5696–5705. [[CrossRef](#)]
38. Liu, X.; Fechner, N.; Antonietti, M. Salt melt synthesis of ceramics, semiconductors and carbon nanostructures. *Chem. Soc. Rev.* **2013**, *42*, 8237. [[CrossRef](#)]
39. Guan, K.; Lei, W.; Wang, H.; Liu, X.; Luo, J.; Liu, J.; Jia, Q.; Zhang, H.; Zhang, S. Efficient synthesis of Ti₃AlC₂ powders with high purity by microwave-assisted molten salt method. *Ceram. Int.* **2022**, *48*, 16357–16363. [[CrossRef](#)]
40. Galvin, T.; Hyatt, N.C.; Rainforth, W.M.; Reaney, I.M.; Shepherd, D. Molten salt synthesis of MAX phases in the Ti-Al-C system. *J. Eur. Ceram. Soc.* **2018**, *38*, 4585–4589. [[CrossRef](#)]
41. Dong, H.; Xiao, P.; Jin, N.; Wang, B.; Liu, Y.; Lin, Z. Molten Salt Derived Nb₂CT_x MXene Anode for Li-Ion Batteries. *Chem. Electrochem.* **2021**, *8*, 957–962.
42. Wang, Y.; Hu, X.; Song, H.; Cai, Y.; Li, Z.; Zu, D.; Zhang, P.; Chong, D.; Gao, N.; Shen, Y.; et al. Oxygen vacancies in actiniae-like Nb₂O₅/Nb₂C MXene heterojunction boosting visible light photocatalytic NO removal. *Appl. Catal. B* **2021**, *299*, 120677. [[CrossRef](#)]
43. Yuan, Z.; Wang, L.; Li, D.; Cao, J.; Han, W. Carbon-Reinforced Nb₂CT_x MXene/MoS₂ Nanosheets as a Superior Rate and High-Capacity Anode for Sodium-Ion Batteries. *ACS Nano* **2021**, *15*, 19. [[CrossRef](#)] [[PubMed](#)]
44. Huang, J.; Wang, M.; Zhang, X.; Tao, J.; Lu, L.; Qiao, G.; Liu, G. Anchoring of 2D CdS on Nb₂CT_x MXene nanosheets for boosting photocatalytic H₂ evolution. *J. Alloy. Compd.* **2022**, *923*, 166256. [[CrossRef](#)]
45. Huang, X.; Zhang, W.; Liu, W.; Zhang, J.; Song, M.; Zhang, C.; Zhang, J.; Wang, D. Nb₂CT_x MXenes functionalized Co–NC enhancing electrochemical H₂O₂ production for organics degradation. *Appl. Catal. B* **2022**, *317*, 121737. [[CrossRef](#)]
46. Fan, X.; Du, P.; Ma, X.; Wang, R.; Ma, J.; Wang, Y.; Fan, D.; Long, Y.; Deng, B.; Huang, K.; et al. Mechanochemical Synthesis of Pt/Nb₂CT_x MXene Composites for Enhanced Electrochemical Hydrogen Evolution. *Materials* **2021**, *14*, 2426. [[CrossRef](#)] [[PubMed](#)]
47. Wu, H.; Xie, Y.; Ma, Y.; Zhang, B.; Xia, B.; Zhang, P.; Qian, W.; He, D.; Zhang, X.; Li, B.W.; et al. Aqueous MXene/Xanthan Gum Hybrid Inks for Screen-Printing Electromagnetic Shielding, Joule Heater, and Piezoresistive Sensor. *Small* **2022**, *18*, 2107087. [[CrossRef](#)]
48. Wang, S.; Jiang, Y.; Liu, B.; Duan, Z.; Pan, H.; Yuan, Z.; Xie, G.; Wang, J.; Fang, Z.; Tai, H. Ultrathin Nb₂CT_x nanosheets-supported polyaniline nanocomposite: Enabling ultrasensitive NH₃ detection. *Sens. Actuators B Chem.* **2021**, *343*, 130069. [[CrossRef](#)]
49. Wang, S.; Liu, B.; Duan, Z.; Zhao, Q.; Zhang, Y.; Xie, G.; Jiang, Y.; Li, S.; Tai, H. PANI nanofibers-supported Nb₂CT_x nanosheets-enabled selective NH₃ detection driven by TENG at room temperature. *Sens. Actuators B Chem.* **2021**, *327*, 128923. [[CrossRef](#)]
50. Khazaei, M.; Ranjbar, A.; Arai, M.; Yunoki, S. Topological insulators in the ordered double transition metals M₂M''C₂ MXenes (M'Mo, W; M''Ti, Zr, Hf). *Phys. Rev. B* **2016**, *94*, 125152. [[CrossRef](#)]
51. Wyatt, C.B.; Rosenkranz, A.; Anasori, B. 2D MXenes: Tunable Mechanical and Tribological Properties. *Adv. Mater.* **2021**, *33*, 2007973. [[CrossRef](#)]
52. Lipatov, A.; Loes, M.J.; Vorobeva, N.S.; Bagher, S.; Abourahma, J.; Chen, H.; Hong, X.; Gogotsi, Y.; Sinitskii, A. High breakdown current density in monolayer Nb₄C₃T_x MXene. *ACS Mater. Lett.* **2021**, *3*, 1088–1094. [[CrossRef](#)]
53. Rahman, U.U.; Humayun, M.; Ghani, U.; Usman, M.; Ullah, H.; Khan, A.; El-Metwaly, N.M.; Khan, A. MXenes as Emerging Materials: Synthesis, Properties, and Applications. *Molecules* **2022**, *27*, 4909. [[CrossRef](#)] [[PubMed](#)]
54. Zhan, X.; Si, C.; Zhou, J.; Sun, Z. MXene and MXene-based composites: Synthesis, properties and environment-related applications. *Nanoscale Horiz.* **2020**, *5*, 235–258. [[CrossRef](#)]
55. Si, C.; Zhou, J.; Sun, Z. Half-Metallic Ferromagnetism and Surface Functionalization-Induced Metal-Insulator Transition in Graphene-Like Two-Dimensional Cr₂C Crystals. *ACS Appl. Mater. Interfaces* **2015**, *7*, 17510–17515. [[CrossRef](#)]

56. Kamysbayev, V.; Filatov, A.S.; Hu, H.; Rui, X.; Lagunas, F.; Wang, D.; Klie, R.F.; Talapin, D.V. Covalent surface modifications and superconductivity of two-dimensional metal carbide MXenes. *Science* **2020**, *369*, 979–983. [[CrossRef](#)]
57. Babar, Z.U.D.; Anwar, M.S.; Mumtaz, M.; Iqbal, M.; Zheng, R.K.; Akinwande, D.; Rizwan, S. Peculiar magnetic behaviour and Meissner effect in two-dimensional layered Nb₂C MXene. *2D Mater.* **2020**, *7*, 035012. [[CrossRef](#)]
58. Din Babar, Z.U.; Fatheema, J.; Arif, N.; Anwar, M.S.; Gul, S.; Iqbal, M.; Rizwan, S. Magnetic phase transition from paramagnetic in Nb₂AlC-MAX to superconductivity-likediamagnetic in Nb₂C-MXene: An experimental and computational analysis. *RSC Adv.* **2020**, *10*, 25669–25678. [[CrossRef](#)]
59. Kumar, P.; Yu, S.; Shahzad, F.; Hong, M.S.; Kim, H.Y.; Koo, M.C. Ultrahigh electrically and thermally conductive self-aligned graphene/polymer composites using large-area reduced graphene oxides. *Carbon* **2016**, *101*, 120–128. [[CrossRef](#)]
60. Liu, S.; Song, Z.; Jin, X.; Mao, R.; Zhang, T.; Hu, F. MXenes for metal-ion and metal-sulfur batteries: Synthesis, properties, and electrochemistry. *Mater. Rep. Energy* **2022**, *2*, 100077. [[CrossRef](#)]
61. Zhang, J.; Kong, N.; Uzun, S.; Levitt, A.; Seyedin, S.; Lynch, P.A.; Qin, S.; Han, M.; Yang, W.; Liu, J.; et al. Scalable Manufacturing of Free-Standing, Strong Ti₃C₂T_x MXene Films with Outstanding Conductivity. *Adv. Mater.* **2020**, *32*, 2001093. [[CrossRef](#)]
62. Xu, J.; Chen, L.; Ding, S.; Dai, X.; Dai, Y.; Chen, Y.; Ni, X. Self-Generated Schottky Barriers in Niobium Carbide MXene Nanocatalysts for Theory-Oriented Sonocatalytic and NIR-II Photonic Hyperthermia Tumor Therapy. *Nano Today* **2023**, *48*, 101750. [[CrossRef](#)]
63. Ramachandran, T.; Thiemann, T.; Hamed, F. Phase evolution and magnetic properties of Dy₃Fe_{5+x}O_{12-x} nanocrystalline powders: A choice of fuel approach. *Mater. Chem. Phys.* **2020**, *240*, 122138. [[CrossRef](#)]
64. Hamed, F.; Ramachandran, T.; Kurapati, V. The effect of induced strains on the optical band gaps in lanthanum doped zinc ferrite nanocrystalline powders. *Mod. Phys. Lett. B* **2016**, *30*, 1650230. [[CrossRef](#)]
65. Zhu, Q.; Li, J.; Simon, P.; Xu, B. Two-dimensional MXenes for electrochemical capacitor applications: Progress, challenges and perspectives. *Energy Storage Mater.* **2021**, *35*, 630–660. [[CrossRef](#)]
66. Lamiel, C.; Hussain, I.; Warner, J.H.; Zhang, K. Beyond Ti-based MXenes: A review of emerging non-Ti based metal-MXene structure, properties, and applications. *Mater. Today* **2023**, *in press*. [[CrossRef](#)]
67. Das, K.; Majumdar, D. Prospects of MXenes/graphene nanocomposites for advanced supercapacitor applications. *J. Electroanal. Chem.* **2022**, *905*, 115973. [[CrossRef](#)]
68. Makola, L.C.; Moeno, S.; Ouma, C.N.; Sharma, A.; Vo, D.-V.N.; Dlamini, L.N. Facile Fabrication of a Metal-Free 2D-2D Nb₂CT_x@g-C₃N₄ MXene-Based Schottky-Heterojunction with the Potential Application in Photocatalytic Processes. *J. Alloy. Compd.* **2022**, *916*, 165459. [[CrossRef](#)]
69. Palisaitis, J.; Persson, I.; Halim, J.; Rosen, J.; Persson, P.O. On the structural stability of MXene and the role of transition metal adatoms. *Nanoscale* **2018**, *10*, 10850–10855. [[CrossRef](#)]
70. Tholkappian, R.; Satheesh Kumar, R.; Mohamed Azarudeen, L.; Anand Kumar, G.; Vishista, K.; Hamed, F. Facile Synthesis of Cr-Doped SrS Phosphor: An Investigations on Structural, Vibrational, Morphological and Photoluminescence Properties. *Mater. Focus* **2016**, *5*, 342–346. [[CrossRef](#)]
71. Echols, I.J.; Holta, D.E.; Kotasthane, V.S.; Tan, Z.; Radovic, M.; Lutkenhaus, J.L.; Green, M.J. Oxidative stability of Nb_{n+1}C_nT_z MXenes. *J. Phys. Chem. C* **2021**, *125*, 13990–13996. [[CrossRef](#)]
72. Zhao, X.; Vashisth, A.; Blivin, J.W.; Tan, Z.; Holta, D.E.; Kotasthane, V.; Shah, S.A.; Habib, T.; Liu, S.; Lutkenhaus, J.L. pH, nanosheet concentration, and antioxidant affect the oxidation of Ti₃C₂T_x and Ti₂CT_x MXene dispersions. *Adv. Mater. Inter.* **2020**, *7*, 2000845. [[CrossRef](#)]
73. Ramachandran, T.; Natarajan, S.; Hamed, F. The role of dysprosium levels in the formation of mixed oxidation states within spinel MnCo_{2-x}Dy_xO₄ nanocrystalline powders. *J. Electron Spectrosc. Relat. Phenom.* **2020**, *242*, 146952. [[CrossRef](#)]
74. Zhu, J.; Lu, X.; Wang, L. Synthesis of a MoO₃/Ti₃C₂T_x composite with enhanced capacitive performance for supercapacitors. *RSC Adv.* **2016**, *6*, 98506–98513. [[CrossRef](#)]
75. Pang, J.; Mendes, G.R.; Bachmatiuk, A.; Zhao, L.; Ta, Q.H.; Gemming, T.; Liu, H.; Liu, Z.; Rummeli, M.H. Applications of 2D MXenes in energy conversion and storage systems. *Chem. Soc. Rev.* **2019**, *48*, 72–133. [[CrossRef](#)] [[PubMed](#)]
76. Luo, W.; Wei, Y.; Zhuang, Z.; Lin, Z.; Li, X.; Hou, C.; Li, T.; Ma, Y. Fabrication of Ti₃C₂T_x MXene/polyaniline composite films with adjustable thickness for high-performance flexible all-solid-state symmetric supercapacitors. *Electrochim. Acta* **2022**, *406*, 139871. [[CrossRef](#)]
77. Naguib, M.; Mashtalir, O.; Carle, J.; Presser, V.; Lu, J.; Hultman, L.; Gogotsi, Y.; Barsoum, W.M. Two-dimensional transition metal carbides. *ACS Nano* **2012**, *6*, 1322–1331. [[CrossRef](#)]
78. Zaheer, A.; Zahra, S.A.; Iqbal, M.Z.; Mahmood, A.; Khand, S.A.; Rizwan, S. Nickel-adsorbed two-dimensional Nb₂C MXene for enhanced energy storage applications. *RSC Adv.* **2022**, *12*, 4624. [[CrossRef](#)] [[PubMed](#)]
79. Xiao, J.; Wen, J.; Zhao, J.; Ma, X.; Gao, H.; Zhang, X. A safe etching route to synthesize highly crystalline Nb₂CT_x MXene for high performance asymmetric supercapacitor applications. *Electrochim. Acta* **2020**, *337*, 135803. [[CrossRef](#)]
80. Raji, R.K.; Ramachandran, T.; Muralidharan, M.; Suriakarthick, R.; Dhilip, M.; Hamed, F.; Kurapati, V. Conventional synthesis of perovskite structured LaTi_xFe_{1-x}O₃: A comprehensive evaluation on phase formation, opto-magnetic, and dielectric properties. *Int. J. Mater. Res.* **2021**, *112*, 753–765. [[CrossRef](#)]
81. Luo, J.; Lu, X.; Matios, E.; Wang, C.; Wang, H.; Zhang, Y.; Hu, X.; Li, W. Tunable MXenederived 1D/2D hybrid nanoarchitectures as a stable matrix for dendrite-free and ultrahigh capacity sodium metal anode. *Nano Lett.* **2020**, *20*, 7700–7708. [[CrossRef](#)]

82. Tholkappiyan, R.; Vishista, K. Tuning the composition and magnetostructure of dysprosium iron garnets by Co-substitution: An XRD, FT-IR, XPS and VSM study. *Appl. Surf. Sci.* **2015**, *351*, 1016–1024. [[CrossRef](#)]
83. Rekha, G.; Tholkappiyan, R.; Vishista, K.; Hamed, F. Systematic study on surface and magnetostructural changes in Mn-substituted dysprosium ferrite by hydrothermal method. *Appl. Surf. Sci.* **2016**, *385*, 171–181. [[CrossRef](#)]
84. Zhang, W.; Jin, H.; Zhang, J. Nb₂CT_x MXene as High-Performance Energy Storage Material with Na, K, and Liquid K–Na Alloy Anodes. *Langmuir* **2021**, *37*, 1102–1109. [[CrossRef](#)] [[PubMed](#)]
85. Ren, X.; Huo, M.; Wang, M.; Lin, H.; Zhang, X.; Yin, J.; Chen, Y.; Chen, H. Highly catalytic niobium carbide (MXene) promotes hematopoietic recovery after radiation by free radical scavenging. *ACS Nano* **2019**, *13*, 6438–6454. [[CrossRef](#)]
86. Yin, J.; Pan, S.; Guo, X.; Gao, Y.; Zhu, D.; Yang, Q.; Gao, J.; Zhang, C.; Chen, Y. Nb₂C MXene-Functionalized Scaffolds Enables Osteosarcoma Phototherapy and Angiogenesis/Osteogenesis of Bone Defects. *Nanomicro Lett.* **2021**, *13*, 30. [[CrossRef](#)]
87. Tan, Y.; Zhu, Z.; Zhang, X.; Zhang, J.; Zhou, Y.; Li, H.; Qin, H.; Bo, Y.; Pan, Z. Nb₄C₃T_x (MXene) as a new stable catalyst for the hydrogen evolution reaction. *Int. J. Hydrog. Energy* **2021**, *46*, 1955–1966. [[CrossRef](#)]
88. Su, T.; Peng, R.; Hood, Z.D.; Naguib, M.; Ivanov, I.N.; Keum, J.K.; Qin, Z.; Guo, Z.; Wu, Z. One-step synthesis of Nb₂O₅/C/Nb₂C (MXene) composites and their use as photocatalysts for hydrogen evolution. *Chem. Sus. Chem.* **2018**, *11*, 688–699. [[CrossRef](#)]
89. Sun, K.Y.; Wu, Y.; Xu, J.; Xiong, W.; Xu, W.; Li, J.; Sun, Z.; Lv, Z.; Wu, X.S.; Jiang, Q.; et al. Niobium carbide (MXene) reduces UHMWPE particle-induced osteolysis. *Bioact. Mater.* **2022**, *8*, 435–448. [[CrossRef](#)]
90. Reding, B.; Carter, P.; Qi, Y.; Li, Z.; Wu, Y.; Wannemuehler, M.; Bratlie, K.M.; Wang, Q. Manipulate intestinal organoids with niobium carbide nanosheets. *J. Biomed. Mater. Res. A* **2021**, *109*, 479–487. [[CrossRef](#)]
91. Song, S.; Liu, J.; Zhou, C.; Jia, Q.; Luo, H.; Deng, L.; Wang, X. Nb₂O₅/Nb₂CT_x composites with different morphologies through oxidation of Nb₂CT_x MXene for high-performance microwave absorption. *J. Alloy. Compd.* **2020**, *843*, 155713. [[CrossRef](#)]
92. Jastrzebska, A.; Szuplewska, A.; Rozmysłowska-Wojciechowska, A.; Mitrzak, J.; Wojciechowski, T.; Chudy, M.; Moszczyńska, D.; Wojcik, A.; Prenger, K.; Naguib, M. Juggling surface charges of 2D niobium carbide mxenes for a reactive oxygen species scavenging and effective targeting of the malignant melanoma cell cycle into programmed cell death. *ACS Sustain. Chem. Eng.* **2020**, *8*, 7942–7951. [[CrossRef](#)]
93. Han, X.; Jing, X.; Yang, D.; Lin, H.; Wang, Z.; Ran, H.; Li, P.; Chen, Y. Therapeutic mesopore construction on 2D Nb₂C MXenes for targeted and enhanced chemo-photothermal cancer therapy in NIR-II biowindow. *Theranostics* **2018**, *8*, 4491–4508. [[CrossRef](#)] [[PubMed](#)]
94. Yang, C.; Luo, Y.; Lin, H.; Ge, M.; Shi, J.; Zhang, X. Niobium carbide MXene augmented medical implant elicits bacterial infection elimination and tissue regeneration. *ACS Nano* **2021**, *15*, 1086–1099. [[CrossRef](#)] [[PubMed](#)]
95. Wang, Z.; Cheng, Z.; Fang, C.; Hou, X.; Xie, L. Recent advances in MXenes composites for electromagnetic interference shielding and microwave absorption. *Compos. A Appl. Sci. Manuf.* **2020**, *136*, 105956. [[CrossRef](#)]
96. Iqbal, A.; Kwon, J.; Kim, M.K.; Koo, C.M. MXenes for electromagnetic interference shielding: Experimental and theoretical perspectives. *Mater. Today Adv.* **2021**, *9*, 100124. [[CrossRef](#)]
97. Rajavel, K.; Yu, X.; Zhu, P.; Hu, Y.; Sun, R.; Wong, C. Investigation on the structural quality dependent electromagnetic interference shielding performance of fewlayer and lamellar Nb₂CT_x MXene nanostructures. *J. Alloy. Compd.* **2021**, *877*, 160235. [[CrossRef](#)]
98. Cui, C.; Guo, R.; Ren, E.; Xiao, H.; Zhou, M.; Lai, X.; Qin, Q.; Jiang, S.; Qin, W. MXene-based rGO/Nb₂CT_x/Fe₃O₄ composite for high absorption of electromagnetic wave. *Chem. Eng. J.* **2021**, *405*, 126626. [[CrossRef](#)]
99. Cui, C.; Guo, R.; Xiao, H.; Ren, E.; Song, Q.; Xiang, C.; Lai, X.; Lan, J.; Jiang, S. Bi₂WO₆/Nb₂CT_x MXene hybrid nanosheets with enhanced visible-lightdriven photocatalytic activity for organic pollutants degradation. *Appl. Surf. Sci.* **2020**, *505*, 144595. [[CrossRef](#)]
100. Peng, C.; Xie, X.; Xu, W.; Zhou, T.; Wei, P.; Jia, J.; Zhang, K.; Cao, Y.; Wang, H.; Peng, F.; et al. Engineering highly active Ag/Nb₂O₅@Nb₂CT_x (MXene) photocatalysts via steering charge kinetics strategy. *Chem. Eng. J.* **2021**, *421*, 128766. [[CrossRef](#)]
101. Yan, P.; Ji, L.; Liu, X.; Guan, Q.; Guo, J.; Shen, Y.; Zhang, H.; Wei, W.; Cui, X.; Xu, Q. 2D amorphous-MoO_{3-x}@Ti₃C₂-MXene non-van der Waals heterostructures as anode materials for lithium-ion batteries. *Nano Energy* **2021**, *86*, 106139. [[CrossRef](#)]
102. Anasori, B.; Lukatskaya, M.R.; Gogotsi, Y. 2D metal carbides and nitrides (MXenes) for energy storage. *Nat. Rev. Mater.* **2017**, *2*, 16098. [[CrossRef](#)]
103. Gao, Y.; Yan, C.; Huang, H.; Yang, T.; Tian, G.; Xiong, D.; Chen, N.; Chu, X.; Zhong, S.; Deng, W.; et al. Microchannel-confined MXene based flexible piezoresistive multifunctional micro-force sensor. *Adv. Funct. Mater.* **2020**, *30*, 1909603. [[CrossRef](#)]
104. Wei, Y.; Soomro, R.A.; Xie, X.; Xu, B. Design of efficient electrocatalysts for hydrogen evolution reaction based on 2D MXenes. *J. Energy Chem.* **2021**, *55*, 244–255. [[CrossRef](#)]
105. Xie, Y.; Naguib, M.; Mochalin, V.N.; Barsoum, M.W.; Gogotsi, Y.; Yu, X.; Nam, K.-W.; Yang, X.-Q.; Kolesnikov, A.I.; Kent, P.R. Role of surface structure on Li-ion energy storage capacity of two-dimensional transition-metal carbides. *J. Am. Chem. Soc.* **2014**, *136*, 6385–6394. [[CrossRef](#)] [[PubMed](#)]
106. Das, P.; Wu, Z.S. MXene for energy storage: Present status and future perspectives. *J. Phys. Energy* **2020**, *2*, 032004. [[CrossRef](#)]
107. Zhang, C.J.; Kremer, M.P.; Seral-Ascaso, A.; Park, S.-H.; McEvoy, N.; Anasori, B.; Gogotsi, Y.; Nicolosi, V. Stamping of flexible, coplanar micro-supercapacitors using MXene inks. *Adv. Funct. Mater.* **2018**, *28*, 1705506. [[CrossRef](#)]
108. Yang, W.; Yang, J.; Byun, J.J.; Moissinac, F.P.; Xu, J.; Haigh, S.J.; Domingos, M.; Bissett, M.A.; Dryfe, R.A.; Barg, S. 3D Printing of Freestanding MXene Architectures for Current-Collector-Free Supercapacitors. *Adv. Mater.* **2019**, *31*, 1902725. [[CrossRef](#)]
109. Jiang, Q.; Kurra, N.; Alhabeib, M.; Gogotsi, Y.; Alshareef, H.N. All pseudocapacitive MXene-RuO₂ Asymmetric supercapacitors. *Adv. Energy Mater.* **2018**, *8*, 1703043. [[CrossRef](#)]

110. Shin, H.; Eom, W.; Lee, K.H.; Jeong, W.; Kang, D.J.; Han, T.H. Highly Electroconductive and Mechanically Strong $\text{Ti}_3\text{C}_2\text{T}_x$ MXene Fibers Using a Deformable MXene Gel. *ACS Nano* **2021**, *15*, 3320–3329. [[CrossRef](#)]
111. VahidMohammadi, A.; Moncada, J.; Chen, H.; Kayali, E.; Orangi, J.; Carrero, C.A.; Beidaghi, M. Thick and freestanding MXene/PANI pseudocapacitive electrodes with ultrahigh specific capacitance. *J. Mater. Chem. A Mater. Energy Sustain.* **2018**, *6*, 22123–22133. [[CrossRef](#)]
112. Vahid Mohammadi, A.; Mojtavavi, M.; Caffrey, M.N.; Wanunu, M.; Beidaghi, M. Assembling 2D MXenes into Highly Stable Pseudocapacitive Electrodes with High Power and Energy Densities. *Adv. Mater.* **2019**, *31*, 1806931. [[CrossRef](#)] [[PubMed](#)]
113. Yu, L.; Hu, L.; Anasori, B.; Liu, Y.-T.; Zhu, Q.; Zhang, P.; Gogotsi, Y.; Xu, B. MXene-Bonded Activated Carbon as a Flexible Electrode for High-Performance Supercapacitors. *ACS Energy Lett.* **2018**, *3*, 1597–1603. [[CrossRef](#)]
114. Zhou, H.; Wu, F.; Fang, L.; Hu, J.; Luo, H.; Guan, T.; Hu, B.; Zhou, M. Layered NiFe-LDH/MXene nanocomposite electrode for high-performance supercapacitor. *Int. J. Hydrog. Energy* **2020**, *45*, 13080–13089. [[CrossRef](#)]
115. Jiang, H.; Wang, Z.; Yang, Q.; Hanif, M.; Wang, Z.; Dong, L.; Dong, M. A novel $\text{MnO}_2/\text{Ti}_3\text{C}_2\text{T}_x$ MXene nanocomposite as high performance electrode materials for flexible supercapacitors. *Electrochim. Acta* **2018**, *290*, 695–703. [[CrossRef](#)]
116. Qian, A.; Hyeon, E.S.; Seo, Y.J.; Chung, H.C. Capacitance changes associated with cation-transport in free-standing flexible $\text{Ti}_3\text{C}_2\text{T}_x$ (TO, F, OH) MXene film electrodes. *Electrochim. Acta* **2018**, *266*, 86–93. [[CrossRef](#)]
117. Xia, Q.X.; Shinde, N.M.; Zhang, T.; Yun, J.M.; Zhou, A.; Mane, R.S.; Mathur, S.; Kim, K.H. Seawater electrolyte-mediated high volumetric MXene-based electrochemical symmetric supercapacitors. *Dalton Trans.* **2018**, *47*, 8676–8682. [[CrossRef](#)]
118. Fu, B.; Sun, J.; Wang, C.; Shang, C.; Xu, L.; Li, J.; Zhang, H. MXenes: Synthesis, Optical Properties, and Applications in Ultrafast Photonics. *Small* **2021**, *17*, 2006054. [[CrossRef](#)]
119. Shein, R.I.; Ivanovskii, L.A. Graphene-like titanium carbides and nitrides $\text{Ti}_{n+1}\text{C}_n$, $\text{Ti}_{n+1}\text{N}_n$ ($n = 1, 2$, and 3) from de-intercalated MAX phases: First-principles probing of their structural, electronic properties and relative stability. *Comput. Mater. Sci.* **2012**, *65*, 104–114. [[CrossRef](#)]
120. Tang, H.; Wang, R.; Shi, L.; Sheremet, E.; Rodriguez, D.R.; Sun, J. Post-processing strategies for improving the electrical and mechanical properties of MXenes. *Chem. Eng. J.* **2021**, *425*, 131472. [[CrossRef](#)]
121. Liu, Y.; Xiao, H.; Goddard, A.W. Schottky-Barrier-Free Contacts with Two-Dimensional Semiconductors by Surface-Engineered MXenes. *J. Am. Chem. Soc.* **2016**, *138*, 15853–15856. [[CrossRef](#)]
122. Hoque, M.M.; Hannan, A.M.; Mohamed, A.; Ayob, A. Battery charge equalization controller in electric vehicle applications: A review. *Renew. Sustain. Energy Rev.* **2017**, *75*, 1363–1385. [[CrossRef](#)]
123. Ghidui, M.; Halim, J.; Kota, S.; Bish, D.; Gogotsi, Y.; Barsoum, W.M. Ion-Exchange and Cation Solvation Reactions in Ti_3C_2 MXene. *Chem. Mater.* **2016**, *28*, 3507–3514. [[CrossRef](#)]
124. Lukatskaya, M.R.; Kota, S.; Lin, Z.; Zhao, M.-Q.; Shpige, N.L.; Levi, M.D.; Halim, J.; Taberna, P.-L.; Barsoum, M.W.; Simon, P.; et al. Ultra-high-rate pseudocapacitive energy storage in two-dimensional transition metal carbides. *Nat. Energy* **2017**, *2*, 17105. [[CrossRef](#)]
125. Anil Kumar, Y.; Koyyada, G.; Ramachandran, T.; Kim, J.H.; Sajid, S.; Moniruzzaman, M.; Alzahmi, S.; Obaidat, I.M. Carbon Materials as a Conductive Skeleton for Supercapacitor Electrode Applications: A Review. *Nanomaterials* **2023**, *13*, 1049. [[CrossRef](#)] [[PubMed](#)]
126. Xie, X.; Zhao, M.-Q.; Anasori, B.; Maleski, K.; Ren, C.E.; Li, J.; Byles, B.W.; Pomerantseva, E.; Wang, G.; Gogotsi, Y. Porous heterostructured MXene/carbon nanotube composite paper with high volumetric capacity for sodium-based energy storage devices. *Nano Energy* **2016**, *26*, 513–523. [[CrossRef](#)]
127. Li, M.; Lu, J.; Luo, K.; Li, Y.; Chang, K.; Chen, K.; Zhou, J.; Rosen, J.; Hultman, L.; Eklund, P.; et al. Element Replacement Approach by Reaction with Lewis Acidic Molten Salts to Synthesize Nanolaminated MAX Phases and MXenes. *J. Am. Chem. Soc.* **2019**, *141*, 4730–4737. [[CrossRef](#)]
128. Zhang, X.; Zhang, Z.; Zhou, Z. MXene-based materials for electrochemical energy storage. *J. Mater. Chem. A Mater. Energy Sustain.* **2018**, *27*, 73–85. [[CrossRef](#)]
129. Hu, M.; Li, Z.; Hu, T.; Zhu, S.; Zhang, C.; Wang, X. High-Capacitance Mechanism for $\text{Ti}_3\text{C}_2\text{T}_x$ MXene by In Situ Electrochemical Raman Spectroscopy Investigation. *ACS Nano* **2016**, *10*, 11344–11350. [[CrossRef](#)]
130. Zhang, C.J.; Nicolosi, V. Graphene and MXene-based transparent conductive electrodes and supercapacitors. *Energy Storage Mater.* **2019**, *16*, 102–125. [[CrossRef](#)]
131. Zhang, P.; Zhu, Q.; Soomro, R.A.; He, S.; Sun, N.; Qiao, N.; Xu, B. In situ ice template approach to fabricate 3D flexible MXene film-based electrode for high performance supercapacitors. *Adv. Funct. Mater.* **2020**, *30*, 2000922. [[CrossRef](#)]
132. De, S.; Acharya, S.; Sahoo, S.; Shim, J.-J.; Nayak, G.C. From 0D to 3D MXenes: Their diverse syntheses, morphologies and applications. *Mater. Chem. Front.* **2022**, *6*, 818–842. [[CrossRef](#)]
133. Wyatt, B.C.; Thakur, A.; Nykiel, K.; Hood, Z.D.; Adhikari, S.P.; Pulley, K.K.; Highland, W.J.; Strachan, A.; Anasori, B. Design of Atomic Ordering in $\text{Mo}_2\text{Nb}_2\text{C}_3\text{T}_x$ MXenes for Hydrogen Evolution Electrocatalysis. *Nano Lett.* **2023**, *23*, 931–938. [[CrossRef](#)] [[PubMed](#)]

Disclaimer/Publisher’s Note: The statements, opinions and data contained in all publications are solely those of the individual author(s) and contributor(s) and not of MDPI and/or the editor(s). MDPI and/or the editor(s) disclaim responsibility for any injury to people or property resulting from any ideas, methods, instructions or products referred to in the content.